

PREPARED FOR SUBMISSION TO JHEP

## Type-X two Higgs doublet model in light of the muon $g - 2$ : confronting Higgs and collider data

---

**Adil Jueid, Jinheung Kim, Soojin Lee, and Jeonghyeon Song**

*Department of Physics, Konkuk University, Seoul 05029, Korea*

*E-mail:* [adil.hep@gmail.com](mailto:adil.hep@gmail.com), [jinheung.kim1216@gmail.com](mailto:jinheung.kim1216@gmail.com),  
[soojinlee957@gmail.com](mailto:soojinlee957@gmail.com), [jhsong@konkuk.ac.kr](mailto:jhsong@konkuk.ac.kr)

**ABSTRACT:** The recent Fermilab measurement of the muon anomalous magnetic moment yields about  $4.2\sigma$  deviation from the SM prediction, when combined with the result of the BNL E821 experiment results. In the Type-X two Higgs doublet model with the Higgs alignment, we study the consequence of imposing the observed muon  $g - 2$ , along with the theoretical stabilities, electroweak oblique parameters, Higgs precision data, and direct searches at the LEP and LHC. For the general study, we scan the whole parameter space and consider two scenarios, the normal scenario where  $h_{\text{SM}} = h$  and the inverted scenario where  $h_{\text{SM}} = H$ , where  $h$  ( $H$ ) is the light (heavy)  $CP$ -even Higgs boson. Extremely large  $\tan\beta$  (above  $\sim 100$ ) and light pseudoscalar mass  $M_A$  to explain the muon  $g - 2$  anomaly make it difficult to maintain the theoretical stability, restricting other masses as  $M_A^2 \simeq M_{H^\pm}^2 \simeq m_{12}^2 \tan\beta \approx M_{h/H}^2$ . Decoupling of new scalar bosons is not possible. The direct search bounds exclude the small  $M_A$  window: crucial is the exotic Higgs decay  $h_{\text{SM}} \rightarrow AA$  in the normal scenario and the LEP  $e^+e^- \rightarrow Ah$  in the inverted scenario. After applying all the constraints, we have narrow mass windows,  $M_A \in [62.5, 145]$  GeV and  $M_H \in [130, 245]$  GeV in the normal scenario while  $M_A \in [70, 105]$  GeV and  $M_h \in [100, 120]$  GeV in the inverted scenario. We also show that the observed electron anomalous magnetic moment is consistent with the model prediction and  $pp \rightarrow Ah/AH$  at the LHC has a high potential to probe the whole surviving parameter space.

---

## Contents

<b>1</b>	<b>Introduction</b>	<b>1</b>
<b>2</b>	<b>Type-X 2HDM</b>	<b>3</b>
<b>3</b>	<b><math>\Delta a_\mu</math> in the Type-X 2HDM</b>	<b>5</b>
<b>4</b>	<b>Theoretical and experimental constraints on the Type-X 2HDM</b>	<b>7</b>
4.1	Scanning strategies in three steps	7
4.2	Results in the normal scenario	8
4.3	Results in the inverted scenario	10
<b>5</b>	<b>Implications on the electron <math>g - 2</math> and the LHC collider signatures</b>	<b>12</b>
5.1	Electron anomalous magnetic moment	12
5.2	Production of the hadro-phobic new scalars at the LHC	13
<b>6</b>	<b>Conclusion</b>	<b>16</b>

---

## 1 Introduction

The recent measurement of the muon anomalous magnetic moment by the Fermilab National Accelerator Laboratory (FNAL) Muon  $g-2$  experiment [1, 2] achieved unprecedented precision as

$$a_\mu^{\text{exp}} = 116\,592\,061(41) \times 10^{-11}, \quad (1.1)$$

where  $a_\mu = (g - 2)_\mu/2$  and the old result of the Brookhaven National Laboratory (BNL) E821 measurement [3] is combined. As the experimental error is becoming comparable with the theoretical error,<sup>1</sup> reliable and accurate calculation of the SM prediction is more important than ever. The recent progress includes five loops in QED [4] and two loops in electroweak interactions [5, 6]. Most dominant is from the strong interaction dynamics at  $\mathcal{O}(1)$  GeV, which is categorized into the hadronic vacuum polarization (HVP) [7–14] and the hadronic light-by-light (HLbL) scattering [15–27]. These QCD corrections cannot be computed using perturbation theory. We have to resort to non-perturbative methods, either Lattice QCD or data-driven ( $R$ -ratio) methods. On the Lattice side, the recent

---

<sup>1</sup>The experimental measurement will be improved in a short time scale. For instance, FNAL will provide a new measurement of  $a_\mu$  in the summer of 2022 after including more data sets.

calculation of the leading order HVP (LO-HVP) contributions to  $a_\mu$  by the Budapest-Marseille-Wuppertal collaboration [28] yields  $a_\mu|_{\text{LO-HVP}} = 707.5(5.3) \times 10^{-10}$ . If we take this result as a face value, the measurement of  $a_\mu$  is consistent with the SM prediction. On the  $R$ -ratio method side, however, the calculation of the HVP contribution [9, 11, 12] supports the long-standing discrepancy between the muon  $g - 2$  experiment and the SM prediction, as

$$\Delta a_\mu = a_\mu^{\text{exp}} - a_\mu^{\text{SM}} = 251(59) \times 10^{-11}. \quad (1.2)$$

The reliability of non-perturbative QCD corrections needs further investigation. One way to check is their connection to electroweak precision fits [29–32]: note that some of the most important inputs to HVP and HLbL contributions come from the measurement of the  $R(s)$ -ratio in  $e^+e^-$  collisions. Lately, some tension is reported between the lattice result and the electroweak data [30, 31]. Another critical topic is finding a proper prescription to combine the probability distribution functions of different errors.

Here we take the  $4.2\sigma$  deviation in Eq. (1.2), which calls for new physics (NP) explanation. In a short time, various NP models have been vigorously studied in light of the muon  $g - 2$ , focusing on a supersymmetric theory [33–45], leptophilic boson model [46, 47], singlet scalar model [48], three Higgs doublet model [49], leptoquark model [50, 51],  $L_\mu - L_\tau$  model [52, 53],  $B - L$  or  $B - 3L$  gauge model [54, 55], flavorful scalar model [56], seesaw model [57], simplified model with minimal field contents [58], effective field theory [59], axion model [60, 61], two Higgs doublet model (2HDM) [62–70], or 2HDM with a singlet scalar model [71]. Although appreciating these early studies, we believe that the research in this direction shall continue. Each NP model which explains the observed  $\Delta a_\mu$  deserves an in-depth study confronting a vast amount of experimental data in particle physics, especially the Higgs precision measurements and new resonance searches at high-energy colliders.

From this motivation, we comprehensively study the  $CP$  invariant Type-X (lepton-specific) 2HDM in light of the  $a_\mu$  anomaly. In the Type-X, the couplings of the new scalar bosons to the SM quarks are suppressed by large  $t_\beta$ , invalidating the hadron-related constraints such as  $B \rightarrow K\mu^+\mu^-$  and  $B_s \rightarrow \mu^+\mu^-$  [72]. We generalize the previous studies of the Type-X 2HDM on  $\Delta a_\mu$  [73–77]. Going beyond cherry-picking specific benchmark points, we scan the whole parameter space of the Type-X 2HDM. Moreover, we take general setting for the Higgs sector, considering two scenarios, the “normal” scenario where the observed Higgs boson is the lighter  $CP$ -even scalar  $h$  and the “inverted” scenario where the heavier  $CP$ -even scalar  $H$  is the observed one. In this general setup, we thoroughly study the impact of the following theoretical and experimental constraints on the model:

- theoretical stabilities such as unitarity, perturbativity, and vacuum stability;
- electroweak precision measurements (through the  $S$ ,  $T$ , and  $U$  parameters);

- Higgs boson signal strength measurements;
- direct searches of new scalars at the LEP, Tevatron, and LHC.

We find that in the Type-X 2HDM, the large and positive  $\Delta a_\mu^{\text{obs}}$  can be explained only by huge  $t_\beta (\gtrsim 100)$  and light pseudoscalar mass  $M_A$ . In this region, the decoupling of the new  $CP$ -even neutral Higgs boson  $\varphi^0$  and the charged Higgs boson  $H^\pm$  is not consistent with the theoretical stability. We will also show that the direct search bounds from the LEP and LHC experiments exclude all the parameter region with  $M_A \lesssim m_{h_{\text{SM}}}/2$ . For future discovery, the LHC process of  $pp \rightarrow A\varphi^0 \rightarrow 4\tau$  is to be suggested as a golden mode to probe the entire parameter space where the observed  $\Delta a_\mu$  is explained, and all the above constraints are satisfied. These are our main results.

The paper is organized in the following way. In Sec. 2, we briefly review the Type-X 2HDM and describe the characteristics of the normal and inverted scenarios in the Higgs alignment limit. In Sec. 3, we discuss the new contributions of the Type-X 2HDM to  $\Delta a_\mu$ , presenting how significantly the observed  $\Delta a_\mu$  affects  $t_\beta$ ,  $M_A$ ,  $M_{H^\pm}$ , and  $m_{\varphi^0}$ . Section 4 describes our strategies for scanning in three steps and shows the results of the allowed parameter space at each step. Section 5 deals with the electron anomalous magnetic moment and the LHC signatures. Conclusions are given in Sec. 6.

## 2 Type-X 2HDM

The 2HDM accommodates two complex  $SU(2)_L$  Higgs doublet scalar fields,  $\Phi_1$  and  $\Phi_2$  [78]:

$$\Phi_i = \begin{pmatrix} w_i^+ \\ \frac{v_i + h_i + i\eta_i}{\sqrt{2}} \end{pmatrix}, \quad i = 1, 2, \quad (2.1)$$

where  $v = \sqrt{v_1^2 + v_2^2} = 246$  GeV. Using the simplified notation of  $s_x = \sin x$ ,  $c_x = \cos x$ , and  $t_x = \tan x$ , we define  $t_\beta = v_2/v_1$ . A discrete  $Z_2$  symmetry under which  $\Phi_1 \rightarrow \Phi_1$  and  $\Phi_2 \rightarrow -\Phi_2$  is imposed in order to prevent the tree-level flavor changing neutral currents [79, 80]. Then the renormalizable and  $CP$  conserving scalar potential with softly broken  $Z_2$  symmetry is

$$\begin{aligned} V_\Phi = & m_{11}^2 \Phi_1^\dagger \Phi_1 + m_{22}^2 \Phi_2^\dagger \Phi_2 - m_{12}^2 (\Phi_1^\dagger \Phi_2 + \text{H.c.}) \\ & + \frac{1}{2} \lambda_1 (\Phi_1^\dagger \Phi_1)^2 + \frac{1}{2} \lambda_2 (\Phi_2^\dagger \Phi_2)^2 + \lambda_3 (\Phi_1^\dagger \Phi_1) (\Phi_2^\dagger \Phi_2) + \lambda_4 (\Phi_1^\dagger \Phi_2) (\Phi_2^\dagger \Phi_1) \\ & + \frac{1}{2} \lambda_5 \left[ (\Phi_1^\dagger \Phi_2)^2 + \text{H.c.} \right], \end{aligned} \quad (2.2)$$

where the  $m_{12}^2$  term softly breaks the  $Z_2$  parity. There are five physical Higgs bosons, the light  $CP$ -even scalar  $h$ , the heavy  $CP$ -even scalar  $H$ , the  $CP$ -odd pseudoscalar  $A$ , and two charged Higgs bosons  $H^\pm$ . The relations of the physical Higgs bosons with the weak

eigenstates in Eq. (2.1) via two mixing angles  $\alpha$  and  $\beta$  are referred to Ref. [81, 82]. Note that the SM Higgs boson is a linear combination of  $h$  and  $H$ , as

$$h_{\text{SM}} = s_{\beta-\alpha}h + c_{\beta-\alpha}H. \quad (2.3)$$

The Yukawa couplings to the SM fermions are written by

$$\begin{aligned} \mathcal{L}_{\text{Yuk}} = & - \sum_f \left( \frac{m_f}{v} y_f^h \bar{f} f h + \frac{m_f}{v} y_f^H \bar{f} f H - i \frac{m_f}{v} y_f^A \bar{f} \gamma_5 f A \right) \\ & - \left\{ \frac{\sqrt{2}}{v} \bar{t} (m_t y_t^A P_L + m_b y_b^A P_R) b H^+ + \frac{\sqrt{2} m_\ell}{v} y_\ell^A \bar{\nu}_\ell P_R \ell H^+ + \text{H.c.} \right\}, \end{aligned} \quad (2.4)$$

where  $P_{R,L} = (1 \pm \gamma^5)/2$  and  $\ell = \mu, \tau$ .

In the Type-X, the observed scalar boson at a mass of 125 GeV is very like the SM Higgs boson, especially in the large  $t_\beta$  limit [83]. Therefore, we take the Higgs alignment limit where one of the  $CP$ -even neutral Higgs bosons is the SM Higgs boson  $h_{\text{SM}}$  [84–88]. There are two ways to realize the Higgs alignment limit, the “normal” and “inverted” scenarios. In the normal scenario, the observed Higgs boson is the lighter  $CP$ -even scalar  $h$ , i.e.,  $s_{\beta-\alpha} = 1$ . In the inverted scenario, the heavier  $CP$ -even scalar  $H$  is the observed one while the lighter one is hidden, wherein the Higgs alignment is satisfied by  $s_{\beta-\alpha} = 0$  [87, 89]. Then the model has five parameters in the physical basis,

$$\{m_{\varphi^0}, M_A, M_{H^\pm}, M^2, t_\beta\} \quad (2.5)$$

where  $M^2 = m_{12}^2/(s_\beta c_\beta)$  and  $\varphi^0$  is the new  $CP$ -even neutral Higgs boson, i.e.,  $\varphi^0 = H$  in the normal scenario and  $\varphi^0 = h$  in the inverted scenario. Two scenarios are summarized as follows:

normal scenario (NS)	inverted scenario (IS)
$h_{\text{SM}} = h, \quad \varphi^0 = H$	$h_{\text{SM}} = H, \quad \varphi^0 = h$
$y_f^{h_{\text{SM}}} = 1, \quad s_{\beta-\alpha} = 1$	$y_f^{h_{\text{SM}}} = 1, \quad s_{\beta-\alpha} = 0$
$y_t^A = -y_t^{\varphi^0} = \frac{1}{t_\beta}, \quad y_\ell^A = y_\ell^{\varphi^0} = t_\beta$	$y_t^A = y_t^{\varphi^0} = \frac{1}{t_\beta}, \quad y_\ell^A = -y_\ell^{\varphi^0} = t_\beta$

(2.6)

In the Higgs alignment limit, the quartic couplings in terms of the model parameters are [90]

$$\begin{aligned} \lambda_1 &= \frac{1}{v^2} \left[ m_{125}^2 + t_\beta^2 (m_{\varphi^0}^2 - M^2) \right], \\ \lambda_2 &= \frac{1}{v^2} \left[ m_{125}^2 + \frac{1}{t_\beta^2} (m_{\varphi^0}^2 - M^2) \right], \\ \lambda_3 &= \frac{1}{v^2} \left[ m_{125}^2 - m_{\varphi^0}^2 - M^2 + 2M_{H^\pm}^2 \right], \\ \lambda_4 &= \frac{1}{v^2} \left[ M^2 + M_A^2 - 2M_{H^\pm}^2 \right], \\ \lambda_5 &= \frac{1}{v^2} \left[ M^2 - M_A^2 \right], \end{aligned} \quad (2.7)$$

where  $m_{125} = 125$  GeV. The second term of  $\lambda_1$  is proportional to  $t_\beta^2$  and thus dominantly controls the theoretical constraints in the limit of large  $t_\beta$ . Therefore, we need the condition of  $m_{\varphi^0}^2 \approx M^2$  to ensure an exact or almost exact cancellation in the  $t_\beta^2$  term of  $\lambda_1$ . This criteria should be satisfied more strictly in the normal scenario where  $m_{\varphi^0} > m_{125}$ . Once we demand  $m_{\varphi^0}^2 \approx M^2$ , the perturbativity of the other quartic couplings,  $|\lambda_{2,\dots,5}| < 4\pi$ , causes a chain reaction of limiting the masses as

$$M_A \sim M_{H^\pm} \sim M \approx m_{\varphi^0}. \quad (2.8)$$

Another smoking-gun signature especially for very light  $M_A$  is the non-SM decay of the Higgs boson,  $h_{\text{SM}} \rightarrow AA$ . The  $h_{\text{SM}}\text{-}A\text{-}A$  vertex is

$$\lambda_{h_{\text{SM}}AA} = \frac{1}{v} (-m_{125}^2 - 2M_A^2 + 2M^2). \quad (2.9)$$

The condition in Eq. (2.8) makes it difficult to have a vanishing  $\lambda_{h_{\text{SM}}AA}$ . Since the Higgs precision measurement puts a strong bound on the exotic Higgs decay as  $\mathcal{B}(h_{\text{SM}} \rightarrow XX) \lesssim \mathcal{O}(0.1)$  [91], the parameter region with  $M_A \leq m_{125}/2$  is highly disfavored.

### 3 $\Delta a_\mu$ in the Type-X 2HDM

The Type-X 2HDM accommodates two kinds of new contributions to  $\Delta a_\mu$ , one-loop contributions and two-loop Barr-Zee contributions [92, 93]. The one-loop contributions are mediated by  $\varphi^0$ ,  $A$ , and  $H^\pm$ , given by [94]

$$\begin{aligned} \Delta a_\mu^{1\text{-loop}} &= \frac{G_F m_\mu^2}{4\pi^2 \sqrt{2}} \sum_\phi (y_\mu^\phi)^2 \rho_\phi^\mu f_\phi(\rho_\phi^\mu) \\ &\simeq 2.6 \times 10^{-15} \sum_\phi (y_\mu^\phi)^2 \left( \frac{100 \text{ GeV}}{M_\phi} \right)^2 f_\phi(\rho_\phi^\mu), \end{aligned} \quad (3.1)$$

where  $\phi = \{\varphi^0, A, H^\pm\}$ ,  $\rho_j^i = m_i^2/m_j^2$ , and the expressions for the loop function  $f_\phi$  are referred to Ref. [94]. The numerical factor in the second equality of Eq. (3.1) implies that the observed  $\Delta a_\mu$  requires very light  $M_\phi$  and/or large  $y_\mu^\phi$ . Because  $\rho_\phi^\mu \ll 1$ , the following asymptotic expansions of the loop functions are useful to understand the behavior of  $\Delta a_\mu^{1\text{-loop}}$ :

$$\begin{aligned} f_{\varphi^0}(\rho) &= -\ln \rho - 7/6 + \mathcal{O}(\rho), \\ f_A(\rho) &= +\ln \rho + 11/6 + \mathcal{O}(\rho), \\ f_{H^\pm}(\rho) &= -1/6 + \mathcal{O}(\rho). \end{aligned} \quad (3.2)$$

Since  $\Delta a_\mu^{1\text{-loop}}$  is proportional to the *square* of  $y_\mu^\phi$ , the contributions of the  $CP$ -even scalar  $\varphi^0$  are positive while those of  $A$  and  $H^\pm$  are negative.

More significant contributions to  $\Delta a_\mu$  are from the two-loop Barr-Zee type diagrams with heavy fermions in the loop [92]:

$$\Delta a_\mu^{\text{BZ}} = \frac{G_F m_\mu^2}{4\pi^2 \sqrt{2}} \frac{\alpha_{\text{em}}}{\pi} \sum_{f, \phi^0} N_f^c Q_f^2 y_\mu^{\phi^0} y_f^{\phi^0} \rho_{\phi^0}^f g_{\phi^0}(\rho_{\phi^0}^f), \quad (3.3)$$

where  $f = t, b, \tau$ ,  $\phi^0 = \{\varphi^0, A\}$ ,  $m_f$ ,  $Q_f$  and  $N_f^c$  are the mass, electric charge and color factor of the fermion  $f$  in the loop, and the loop functions are

$$g_{\varphi^0}(r) = \int_0^1 dx \frac{2x(1-x) - 1}{x(1-x) - r} \ln \frac{x(1-x)}{r}, \quad (3.4)$$

$$g_A(r) = \int_0^1 dx \frac{1}{x(1-x) - r} \ln \frac{x(1-x)}{r}.$$

For the top quark and  $\tau^\pm$  loops, the factor  $\rho_{\phi^0}^f (= m_f^2/m_{\phi^0}^2)$  in Eq. (3.3) significantly enhances  $\Delta a_\mu^{\text{BZ}}$  with respect to  $\Delta a_\mu^{1\text{-loop}}$  in Eq. (3.1). The usual consequence that a  $CP$ -even ( $CP$ -odd) scalar boson makes negative (positive) contribution to  $\Delta a_\mu^{\text{BZ}}$  holds true when  $y_\mu^\phi y_f^\phi > 0$ . As can be seen from Eq. (2.6), the top quark contributions mediated by the  $CP$ -even  $\varphi^0$  in both scenarios incorporate  $y_\mu^{\varphi^0} y_t^{\varphi^0} < 0$  and thus generate *positive* two-loop Barr-Zee contributions.

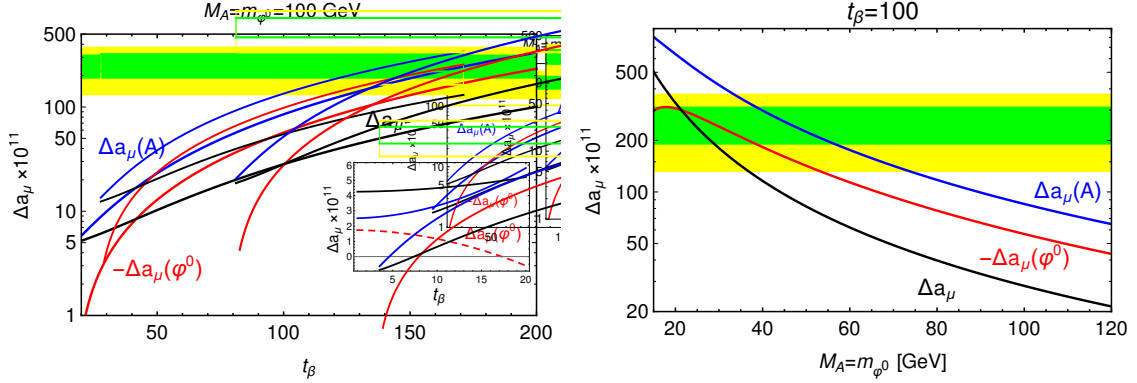


**Figure 1:**  $\Delta a_\mu$  from  $A$ ,  $-\Delta a_\mu$  from  $\varphi^0$ , and  $\Delta a_\mu(A) + \Delta a_\mu(\varphi^0)$  as a function of  $t_\beta$  with  $M_A = m_{\varphi^0} = 100$  GeV (left panel) and as a function of  $M_A = m_{\varphi^0}$  for  $t_\beta = 100$  (right panel).

In Fig. 1, we show  $\Delta a_\mu(A)$  (blue line),  $-\Delta a_\mu(\varphi^0)$  (red line), and  $\Delta a_\mu(A) + \Delta a_\mu(\varphi^0)$  (black line)<sup>2</sup> as a function of  $t_\beta$  with  $M_A = m_{\varphi^0} = 100$  GeV in the left panel and as a function of  $M_A = m_{\varphi^0}$  for  $t_\beta = 100$  in the right panel. To show negative value of  $\Delta a_\mu(\varphi^0)$  in the logarithmic scale, we present  $-\Delta a_\mu(\varphi^0)$ . The allowed region of  $\Delta a_\mu$  at  $1\sigma$  ( $2\sigma$ ) by the measurement in Eq. (1.2) is the horizontal green (yellow) area. The dominant contribution of  $A$  is from the two-loop Barr-Zee diagram, which is always positive and rapidly increasing with increasing  $t_\beta$ . The contribution of  $\varphi^0$  is negative for very large  $t_\beta$

<sup>2</sup>This total  $\Delta a_\mu$  is for illustration, since it holds true only for  $M_A = m_{\varphi^0}$ .

since the  $\tau$  loop contribution in the two-loop Barr-Zee diagram is prevailing. In order to see the behavior of  $\Delta a_\mu(\varphi^0)$  for a moderate value of  $t_\beta$ , we present  $\Delta a_\mu$  for  $t_\beta \in [1, 20]$  in the small figure inside the left panel. If  $t_\beta \lesssim 17$ , dominant contribution mediated by the  $CP$ -even  $\varphi^0$  is from the top quark loop in the two-loop Barr-Zee diagram, which is positive due to  $y_\mu^{\varphi^0} y_t^{\varphi^0} < 0$ . Although both contributions from  $A$  and  $\varphi^0$  are positive, the absolute value of  $\Delta a_\mu$  is not enough to explain  $\Delta a_\mu^{\text{obs}}$ . In the right panel, we show  $\Delta a_\mu(A)$  and  $-\Delta a_\mu(\varphi^0)$  as a function of  $M_A = m_{\varphi^0}$  by fixing  $t_\beta = 100$ .  $\Delta a_\mu$  increases very rapidly with decreasing scalar mass. Since the negative contributions of the  $CP$ -even  $\varphi^0$  become severe with decreasing  $m_{\varphi^0}$ , the inverted scenario receives stronger constraint.

## 4 Theoretical and experimental constraints on the Type-X 2HDM

### 4.1 Scanning strategies in three steps

In light of the observed  $\Delta a_\mu$ , we comprehensively study the Type-X 2HDM, confronting the theoretical and experimental constraints. For the model parameters in Eq. (2.5), we perform the successive and cumulative scan in three steps. We obtained  $5 \times 10^5$  parameter sets for each scenario that satisfy the Step II constraints. After applying the Step III constraints, about  $10^5$  parameter sets survive in the normal scenario: Step III excludes about 80% of the parameter sets that survive Step II. In the inverted scenario, only  $\sim 1.8\%$  parameter sets survive.

#### Step I: Anomalous magnetic moment of the muon

We demand that the model explains the observed  $\Delta a_\mu$  at  $2\sigma$ .

#### Step II: Theory+EWPD after Step I

1. Theoretical stabilities [87, 95, 96]
  - Higgs potential being bounded from below [96];
  - Unitarity of scalar-scalar scatterings [78, 97];
  - Perturbativity [87];
  - Vacuum stability [95].
2. Peskin-Takeuchi electroweak oblique parameters [98]

We take the current best-fit results of [98]

$$\begin{aligned}
S &= -0.01 \pm 0.10, & T &= 0.03 \pm 0.12, & U &= 0.02 \pm 0.11, & (4.1) \\
\rho_{ST} &= 0.92, & \rho_{SU} &= -0.80, & \rho_{TU} &= -0.93,
\end{aligned}$$

where  $\rho_{ij}$  is the correlation matrix. The expressions of the contributions from the scalar boson loops to  $S/T/U$  are referred to Ref. [99, 100]. We require  $\Delta\chi^2 (= \chi^2 - \chi_{\text{min}}^2) < 7.81$ .

### Step III: Collider bounds after Step II

1. Higgs precision data by using `HiggsSignals` [101, 102]:

The `HiggsSignals-v2.2.0` [102] yields a  $\chi^2$  value for 107 Higgs observables. Since our model has five parameters in Eq. (2.5), the number of degrees of freedom for the  $\chi^2$  analysis is 102. We demand that the calculated Higgs signal strengths are consistent with the experimental measurements at  $2\sigma$  level.

2. Direct searches for new scalars at the LEP, Tevatron, and LHC:

We use `HiggsBounds` [103]. Main search channels which affect the Type-X 2HDM are found to be

- LEP experiments:
  - $e^+e^- \rightarrow Z \rightarrow Ah \rightarrow \tau^+\tau^-\tau^+\tau^-$  [104]
- LHC experiments:
  - $h \rightarrow AA$  [105–110],
  - $H \rightarrow ZZ/W^+W^-$  [111–113]
  - $H \rightarrow hh$  [111, 114–120];
  - $H/A \rightarrow \gamma\gamma$  [121, 122],  $\tau^+\tau^-$  [123, 124],  $\mu^+\mu^-$  [125–127],  $b\bar{b}$  [128–130],  $t\bar{t}$  [131];
  - $A \rightarrow Zh$  [132, 133];
  - $A(H) \rightarrow ZH(A)$  [134, 135];
  - $H^\pm \rightarrow tb$  [136, 137],  $\tau^\pm\nu$  [138, 139].

In our analysis, we computed the  $r_{95\%}$  defined by

$$r_{95\%} = \frac{S_{2\text{HDM}}}{S_{\text{obs}}^{95\%}}, \quad (4.2)$$

where  $S_{2\text{HDM}}$  ( $S_{\text{obs}}^{95\%}$ ) is the predicted (observed) cross section. A point in the parameter space is excluded at the 95% confidence level if  $r_{95\%} > 1$ .

## 4.2 Results in the normal scenario

We show the allowed  $(M_A, t_\beta)$  of the normal scenario in Fig. 2, following the sequence of three steps in the previous subsection. At Step I (the left panel), which demands to explain only the  $\Delta a_\mu^{\text{obs}}$ , intermediate  $M_A$  as well as very heavy  $M_H$  and  $M_{H^\pm}$  up to  $\mathcal{O}(1)$  TeV are allowed. At Step II (middle panel), a considerable reduction of the allowed parameter space occurs. This is because the theoretical stability strongly prefers  $M_A \sim M_{H^\pm} \sim M_H (\approx M)$  as discussed in Eq. (2.8): the effects of the Peskin-Takeuchi oblique parameters are mild. Both  $M_H$  and  $M_{H^\pm}$  cannot be too heavy. In Fig. 3, we show the allowed  $M_H$  and  $M_{H^\pm}$  at the final Step III, with the color code of  $\Delta a_\mu$ . There exist upper bounds on the heavy scalar bosons:  $M_H \leq 245$  GeV and  $M_{H^\pm} \leq 285$  GeV. Besides, there is no correlation of

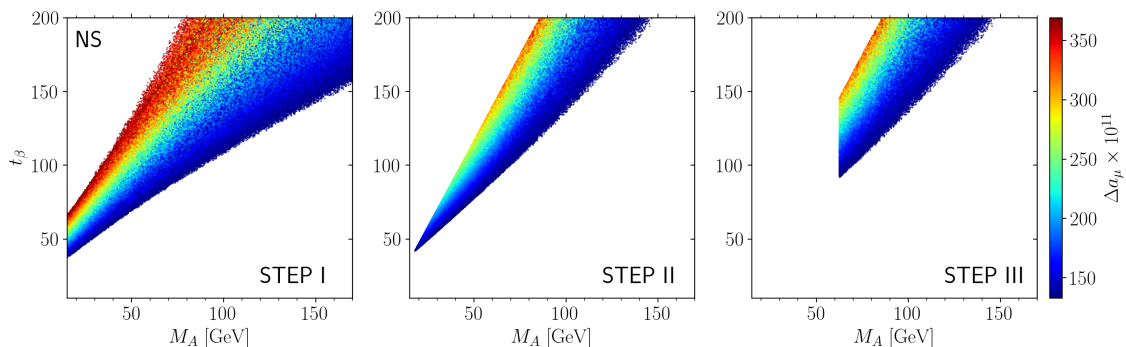


**Figure 2:** In the normal scenario, the allowed parameter space of  $(M_A, t_\beta)$  after Step I ( $\Delta a_\mu^{\text{obs}}$ ), Step II (Step I+Theory+EWPD), and Step III (Step II+Collider), with the color code indicating the value of  $\Delta a_\mu$ .

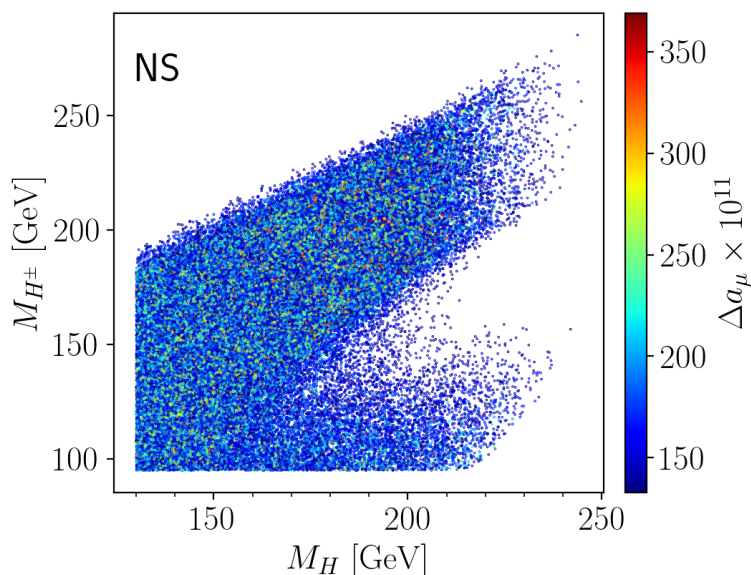


**Figure 3:** The allowed  $(M_H, M_{H^\pm})$  in the normal scenario at Step III. The color code indicates the value of  $\Delta a_\mu$ .

$\Delta a_\mu$  with  $M_H$  or  $M_{H^\pm}$  as indicated by the mixed colors. As only the intermediate-mass  $H$  survives, the negative contribution of  $H$  becomes significant and lowers the total  $\Delta a_\mu$ . Therefore, only  $M_A < 145$  GeV can explain the observed  $\Delta a_\mu$ . If we demand the central value of  $\Delta a_\mu^{\text{obs}}$ , the pseudoscalar boson should be lighter like  $M_A \leq 100$  GeV.

At the final step (Step III) in the normal scenario, the whole parameter space of  $M_A < m_{125}/2$  is removed, which requires  $t_\beta \gtrsim 90$  in turn. A vital question is which collider processes exclude the region with  $M_A < m_{125}/2$ . Usually, several different processes prohibit one parameter set. For efficient illustration, we present in Fig. 4 only the smoking-

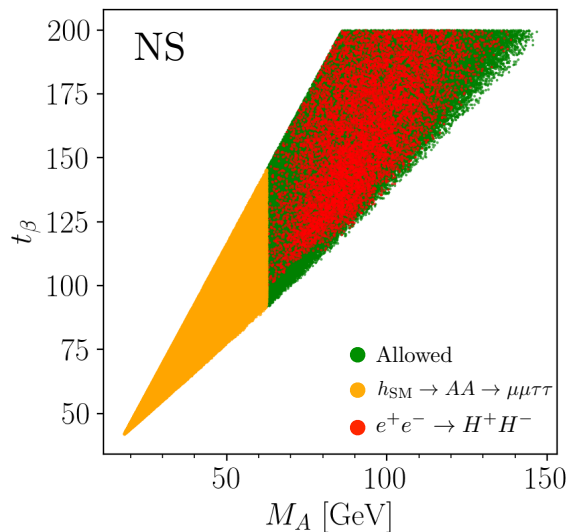


**Figure 4:** In the normal scenario at Step III, the allowed points (green) and the excluded points (orange and red) in the parameter space of  $(M_A, t_\beta)$ . The orange points are excluded by  $h_{\text{SM}} \rightarrow AA \rightarrow \mu^+\mu^-\tau^+\tau^-$  at the LHC, while the red points are excluded by  $e^+e^- \rightarrow H^+H^-$  at the LEP.

gun process, which has the largest deviation of the model prediction from the observation,  $r_{95\%}$  in Eq. (4.2). The green points pass the final step. The orange points are excluded by the LHC bounds on  $h_{\text{SM}} \rightarrow AA \rightarrow \mu^+\mu^-\tau^+\tau^-$  [107, 140]. There was an observation that the opposite-sign tau lepton Yukawa coupling to the SM Higgs boson, which is realized by  $c_{\beta-\alpha} = 2/t_\beta$  [94], may suppress the non-SM decay of  $h_{\text{SM}} \rightarrow AA$ . However, we found that the theoretical stability conditions are too strong to suppress  $\lambda_{h_{\text{SM}}AA}$  in Eq. (2.9) even for  $y_\tau^{h_{\text{SM}}} = -1$ . The red points are excluded by the LEP process  $e^+e^- \rightarrow H^+H^-$  where all of the four LEP experiment results are combined by including the decays of the charged Higgs boson pair into  $c\bar{s}c\bar{s}$ ,  $c\bar{s}\tau\nu$ ,  $\tau\nu\tau\nu$ ,  $W^*A\tau\nu$ , and  $W^*AW^*A$  [141]. The overlap of the allowed (green) points and the excluded (red) points in Fig. 4 is attributed to our projection of five-dimensional points onto two-dimensional  $(M_A, t_\beta)$  plane. In summary, the final Step III (the right panel of Fig. 2) implies that the observed  $\Delta a_\mu$  can be explained by  $t_\beta \gtrsim 90$  and  $M_A \in [62.5, 145]$  GeV when scanning  $t_\beta$  up to 200.

### 4.3 Results in the inverted scenario

In the inverted scenario, the overall behavior of the allowed parameter space is similar to that in the normal scenario: see Fig. 5. In the quantitative aspect, however, there are significant differences. At Step I, the observed  $\Delta a_\mu$  prefers lighter  $M_A$  than in the normal scenario, as the lighter  $h$  makes a sizably negative contribution. The constraints at Step II are weaker than in the normal scenario. The perturbativity of  $\lambda_1$ , the most critical factor for the theoretical stability, is easier to satisfy with light  $m_{\varphi^0} (= M_h)$ . We also observe that the allowed parameter points at Step I and Step II have mixed colors, implying that

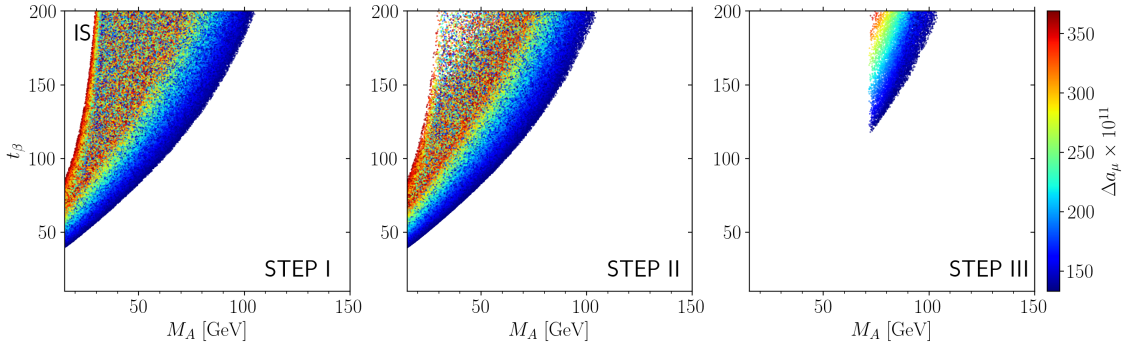


**Figure 5:** In the inverted scenario, the allowed parameter space of  $(M_A, t_\beta)$  at Step I, Step II, and Step III, with the color code indicating the value of  $\Delta a_\mu$ .

the correlation of  $\Delta a_\mu$  with  $M_A$  or  $t_\beta$  at Step II is weak.

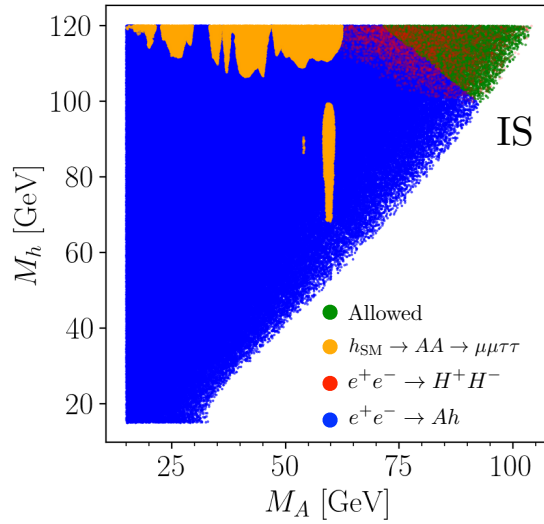


**Figure 6:** In the inverted scenario at the final Step III, the allowed points (green) and the excluded points (orange, red, and blue). The orange points are excluded by  $h_{\text{SM}} \rightarrow AA \rightarrow \mu^+\mu^-\tau^+\tau^-$  at the LHC, the red points by  $e^+e^- \rightarrow H^+H^-$  at the LEP, and the blue points by  $e^+e^- \rightarrow Ah$  at the LEP.

The collider constraints in the inverted scenario (the right panel of Fig. 5) are much stronger than in the normal scenario. As discussed in Sec. 4.1, only  $\sim 1.8\%$  of the allowed points at Step II survive Step III in the inverted scenario: in the normal scenario, it is about 20%. Only extraordinarily large  $t_\beta$  is allowed,  $t_\beta \gtrsim 120$ . At Step III, there exists the correlation of  $\Delta a_\mu$  with  $M_A$  and  $t_\beta$ , as can be seen from unblended colors. Figure 6 presents the smoking-gun process which yields the largest deviation of the model prediction from the observation. Green points are finally allowed, orange points are excluded by  $h_{\text{SM}} \rightarrow AA$  [107, 140], and red points by the LEP process  $e^+e^- \rightarrow H^+H^-$  [141]. A new

killing process is the LEP process of  $e^+e^- \rightarrow Z^* \rightarrow Ah$  [104], denoted by blue points. The effect of this process is dominant since the  $Z$ - $A$ - $h$  vertex of the gauge coupling origin is proportional to  $c_{\beta-\alpha}$ , which is maximal in the alignment limit of the inverted scenario. We found that the constraint is so strong that only the kinematic ban of  $\sqrt{s_{ee}} < M_A + M_h$  saves the parameter space.

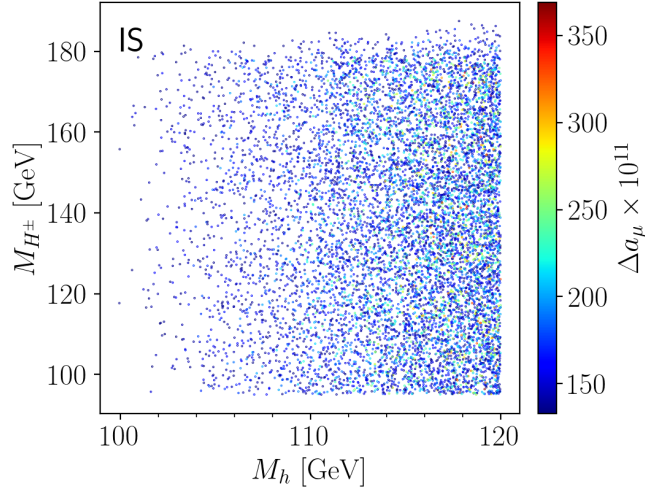


**Figure 7:** The finally allowed  $(M_h, M_{H^\pm})$  in the inverted scenario with the color code indicating the value of  $\Delta a_\mu$ .

In Fig. 7, we present the finally allowed  $(M_h, M_{H^\pm})$  in the inverted scenario with the color code indicating the value of  $\Delta a_\mu$ . As in the normal scenario, there is no correlation of  $\Delta a_\mu$  with  $M_h$  or  $M_{H^\pm}$ : see the mixed color distribution. On the contrary, we have a stronger bound on the mass of the charged Higgs boson:  $M_{H^\pm} \in [95, 190]$  GeV.

## 5 Implications on the electron $g - 2$ and the LHC collider signatures

### 5.1 Electron anomalous magnetic moment

As a flavor-universal theory, the Type-X 2HDM has the same contributions to the electron  $g - 2$  as to the muon  $g - 2$ , apart from the differences of the electron and muon masses. If the muon  $g - 2$  deviates from the SM prediction, the electron  $g - 2$  should do. Furthermore, positive  $\Delta a_\mu$  demands positivity of  $\Delta a_e$  in the Type-X 2HDM. Therefore, it is essential to study the prediction of the finally allowed parameter points to the electron anomalous magnetic moment.

The measurement of the electron magnetic moment [142] is sensitive to the value of the fine structure constant  $\alpha$ , which depends on whether we take the data from  $^{133}\text{Cs}$  [143] or from  $^{87}\text{Rb}$  [144]. The deviations of the electron  $g - 2$  from the SM prediction [145, 146]

according to two different  $\alpha$  values are [46]

$$\begin{aligned}\Delta a_e^{\text{Cs}} &= -8.8(3.6) \times 10^{-13}, \\ \Delta a_e^{\text{Rb}} &= 4.8(3.0) \times 10^{-13}.\end{aligned}\tag{5.1}$$

At  $2\sigma$  level,  $\Delta a_e^{\text{Cs}}$  is negative while  $\Delta a_e^{\text{Rb}}$  can be positive.

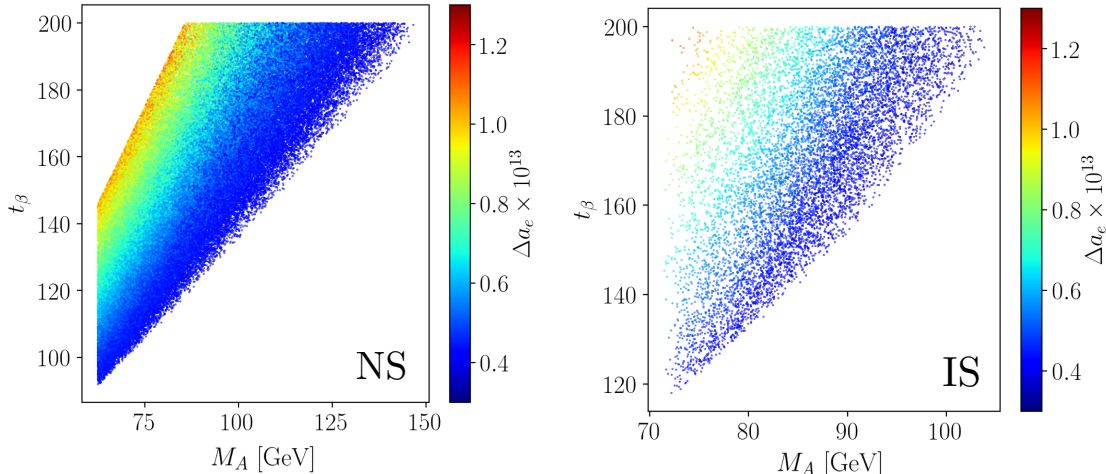


**Figure 8:**  $\Delta a_e$  of the finally allowed parameter points that satisfy all the theoretical and experimental constraints including  $\Delta a_\mu$ , projected on  $(M_A, t_\beta)$ . The left (right) panel corresponds to the normal (inverted) scenario.

In Fig. 8, we present the  $\Delta a_e$  of the finally allowed parameter points that satisfy all the theoretical and experimental constraints including  $\Delta a_\mu$ , projected on  $(M_A, t_\beta)$ . The left (right) panel corresponds to the normal (inverted) scenario. In both scenarios, the phenomenologically reliable parameter sets predict  $\Delta a_e \in [0.36, 1.17] \times 10^{-13}$  in the normal scenario and  $\Delta a_e \in [0.33, 1.15] \times 10^{-13}$  in the inverted scenario. The observed  $\Delta a_e^{\text{Rb}}$  is explained at  $2\sigma$ , except for the points along the upper-left boundary of the allowed space. The negativity of the observed  $\Delta a_e^{\text{Cs}}$  at  $2\sigma$  is contradictory to the  $\Delta a_e$  predicted in the Type-X 2HDM. At  $3\sigma$ , however,  $\Delta a_e$  in our model is consistent with  $\Delta a_e^{\text{Cs}}$ .

## 5.2 Production of the hadro-phobic new scalars at the LHC

Essential results of our comprehensive study of the Type-X 2HDM in light of new measurement of  $\Delta a_\mu$  are arranged in two ways: (i)  $t_\beta$  is extremely large,  $t_\beta \gtrsim 90$  in the normal scenario and  $t_\beta \gtrsim 120$  in the inverted scenario; (ii) the masses of new scalar bosons are bounded from above, all being below  $\lesssim 300$  GeV. As new scalar bosons are within reach of the LHC, the implications on their signatures at the LHC as well as future colliders [147] are of great significance.

We begin the study with the question of how such a light  $M_{H^\pm}$  is allowed by the existing searches for the charged Higgs bosons at the LHC. Note that the current LHC

search for a light charged Higgs boson depends on the production via the decay of a top quark into  $bH^\pm$ , followed by  $H^\pm \rightarrow \tau\nu$  [138, 139]. For  $t_\beta \gtrsim 120$ , new scalar bosons become hadro-phobic [148, 149] and thus  $\mathcal{B}(t \rightarrow bH^\pm)$  is extremely suppressed. The process of  $pp \rightarrow t\bar{t}(t \rightarrow bH^\pm)$  is not efficient to probe the light  $H^\pm$ . The LHC searches for new neutral scalar bosons,  $A$  and  $\varphi^0$ , depend on the gluon fusion production via top quark loops, which is also suppressed. These hadro-phobic new scalar bosons require different search strategies.

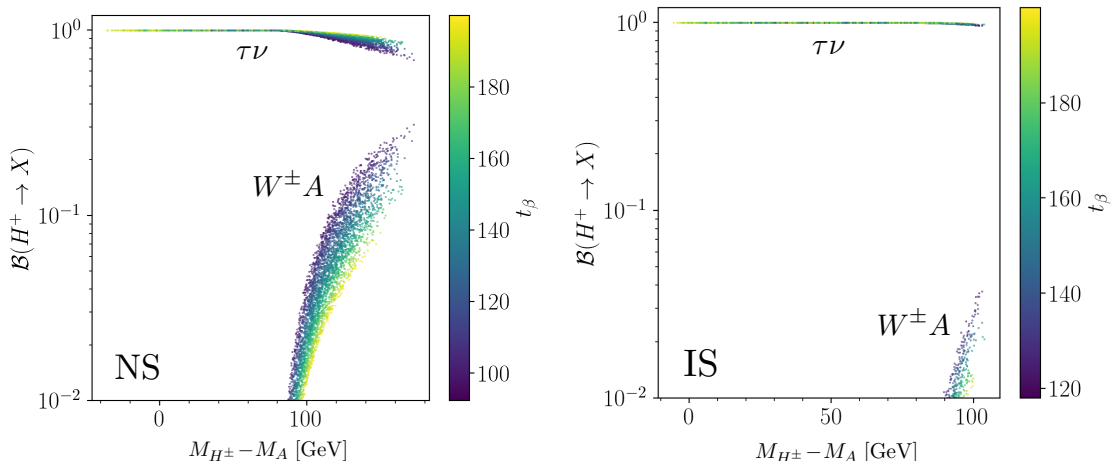


**Figure 9:** The branching ratios of the charged Higgs boson as a function of  $M_{H^\pm} - M_A$  for the finally allowed parameter points. The left (right) panel corresponds to the normal (inverted) scenario.

We study the branching ratios of  $A$ ,  $\varphi^0$ , and  $H^\pm$  in the finally allowed parameter space including  $\Delta a_\mu$ . We found that both  $A$  and  $\varphi^0$  dominantly decay into  $\tau^+\tau^-$ . Possibly important decay modes,  $H \rightarrow ZA$  and  $H \rightarrow H^\pm W^\mp$ , have the branching ratios below 10%. The primary decay channel of the charged Higgs boson is into  $\tau^\pm\nu$ . The other significant mode is  $H^\pm \rightarrow W^\pm A$ , which depends sensitively on the mass difference between  $M_{H^\pm}$  and  $M_A$ . Figure 9 shows the branching ratios of  $H^\pm$  as a function of  $M_{H^\pm} - M_A$  over the finally surviving parameter points. The color code indicates the value of  $t_\beta$ . In the normal scenario (left panel),  $H^\pm \rightarrow W^\pm A$  becomes sizable for larger  $M_{H^\pm} - M_A \gtrsim 100$  GeV and smaller  $t_\beta$ . The branching ratio can reach up to about 30%. In the inverted scenario (right panel),  $\mathcal{B}(H^\pm \rightarrow W^\pm A)$  shows similar behavior to that in the normal scenario but its magnitude is much smaller: the maximum is about 3%. In summary, the hadron-phobic Type-X 2HDM suggests the search channels resorting to the decays of  $A/\varphi^0 \rightarrow \tau^+\tau^-$  and  $H^\pm \rightarrow \tau^\pm\nu$ , i.e., the multi- $\tau$  signatures [150].

Considering the above characteristic features, we consider the following two channels:

$$q\bar{q} \rightarrow Z^* \rightarrow A\varphi^0 \rightarrow \tau^+\tau^-\tau^+\tau^-, \quad (5.2)$$

$$pp \rightarrow H^+H^- \rightarrow \tau^+\nu\tau^-\nu, \quad (5.3)$$

where  $\varphi^0 = H (h)$  in the normal (inverted) scenario. The process in Eq. (5.2) is very efficient since the  $Z$ - $A$ - $\varphi^0$  vertex has the maximal value in the alignment limit of both scenarios. In addition, the mass of the  $CP$ -even neutral scalar  $\varphi^0$  can be known through the  $\tau^+\tau^-$  invariant mass distribution, differentiating the normal scenario from the inverted scenario. The production cross section of the process in Eq. (5.3) is almost uniquely determined by  $M_{H^\pm}$  since the production is via the gauge couplings to  $\gamma$  and  $Z$ . The ambiguity from the other model parameters is minor. The exact calculation of the significances of two processes in Eq. (5.2) and (5.3) requires the full detector-level simulation, incorporating the tagging and mistagging efficiencies of  $\tau$  leptons with low  $p_T$ . Since full simulations scanning the whole allowed parameter space are beyond the scope of this paper, we calculate the total cross sections of new signals at the parton-level and compare them with the irreducible backgrounds.

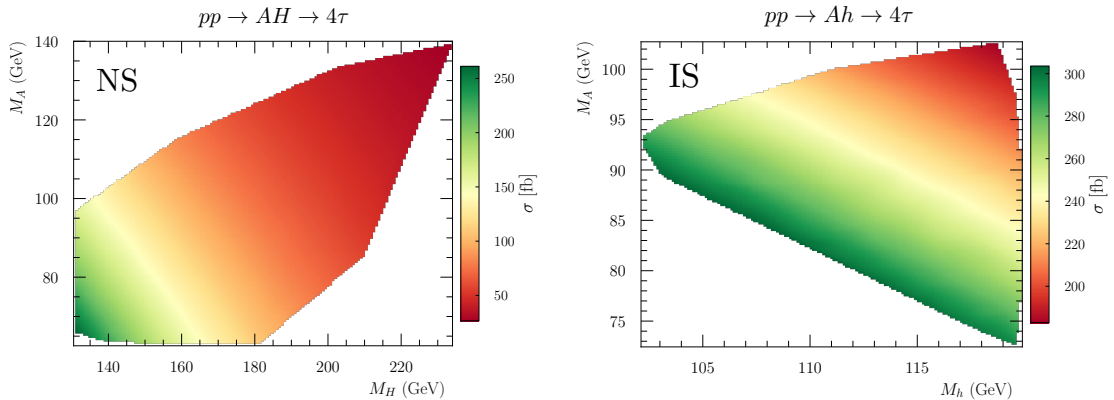


**Figure 10:** The total cross section at the 14 TeV LHC for the process  $pp \rightarrow Z^* \rightarrow AH/Ah \rightarrow 4\tau$  of the finally allowed parameter points, projected on  $(M_H/M_h, t_\beta)$ . The left (right) panel corresponds to the normal (inverted) scenario.

Figure 10 shows total cross section at the 14 TeV LHC for the process  $pp \rightarrow Z^* \rightarrow AH/Ah \rightarrow 4\tau$  of the finally allowed parameter points, projected on  $(M_H/M_h, t_\beta)$ . In the normal scenario (left panel) where  $M_H$  can reach up to  $\sim 235$  GeV, the total cross section lies between  $\sim 25$  fb and  $\sim 260$  fb. We see a strong correlation of  $\sigma_{\text{tot}}$  with  $M_A + M_H$ : the smaller  $M_A + M_H$  is, the larger  $\sigma_{\text{tot}}$  is. In the inverted scenario where  $M_h$  is generically less than  $m_{125}$ , the absolute value of  $\sigma_{\text{tot}}$  is larger than that in the normal scenario. It can reach about 300 fb. The irreducible background of  $pp \rightarrow ZZ \rightarrow 4\tau$  is observed with the total cross section of  $\sim 17$  fb at the 13 TeV LHC [151, 152]. Therefore, the process  $pp \rightarrow A\varphi^0 \rightarrow 4\tau$  has a high potential to probe the whole allowed parameter space of the Type-X 2HDM.

In Fig. 11, we present the total cross section at the 14 TeV LHC for the process  $pp \rightarrow H^+H^- \rightarrow \tau\nu\tau\nu$  of the finally allowed parameter points, projected on the  $(M_{H^\pm}, t_\beta)$  plane. The results in the normal (inverted) scenario are in the left (right) panel. Two

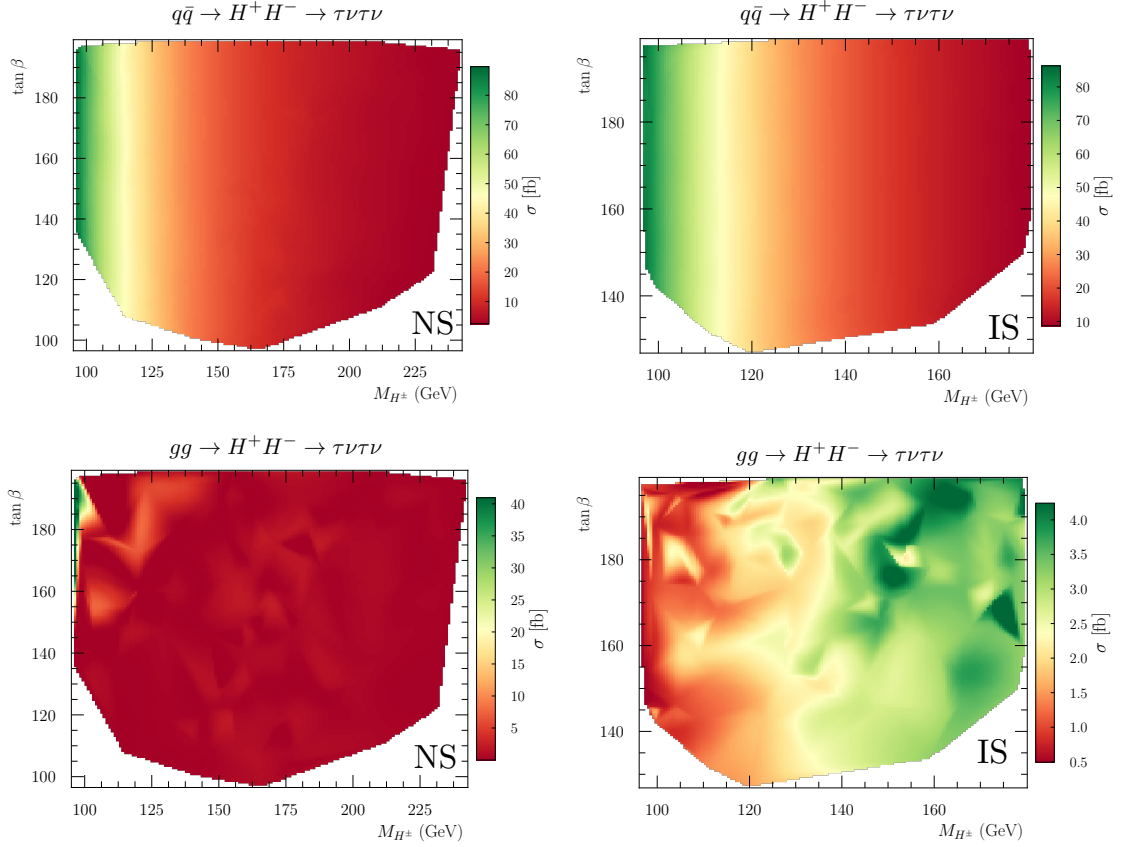


**Figure 11:** The total cross section at the 14 TeV LHC for the process  $pp \rightarrow H^+H^- \rightarrow \tau\nu\tau\nu$  of the finally allowed parameter points, projected on  $(M_{H^\pm}, t_\beta)$ . The results in the normal (inverted) scenario are in the left (right) panels. Two upper panels correspond to  $q\bar{q} \rightarrow H^+H^-$ , and two lower panels to the gluon fusion production.

upper panels present the total cross section for  $q\bar{q} \rightarrow H^+H^-$ , and two lower panels for the gluon fusion production. In most parameter space, the Drell-Yan production has a much larger signal rate, since the hadro-phobic nature of the charged Higgs boson suppresses the gluon fusion production mediated by the top quark loop. The color distributions in the two upper panels show that  $M_{H^\pm}$  practically determines  $\sigma_{\text{tot}}(q\bar{q} \rightarrow H^+H^-)$  since its production is via gauge interactions. The irreducible backgrounds for the final state of  $\tau\nu\tau\nu$  are from  $pp \rightarrow W^+W^- \rightarrow \tau\nu\tau\nu$  and  $pp \rightarrow ZZ \rightarrow \tau^+\tau^-\nu\nu$ . Considering  $\sigma_{\text{tot}}^{\text{SM}}(pp \rightarrow W^+W^- \rightarrow \tau\nu\tau\nu) \simeq 1.7$  pb [153] and  $\sigma_{\text{tot}}^{\text{SM}}(pp \rightarrow ZZ \rightarrow \tau^+\tau^-\nu\nu) \simeq 100$  fb [151, 152] at the 13 TeV LHC, there is a chance of probing  $pp \rightarrow H^+H^- \rightarrow \tau\nu\tau\nu$  if we increase the signal significance to a certain extent.

## 6 Conclusion

In light of the recent measurement of the muon anomalous magnetic moment by Fermilab Muon  $g-2$  experiment, we comprehensively study the Type-X (Lepton-specific) two Higgs

doublet model (2HDM). Beyond explaining the observed  $\Delta a_\mu$  only, we included in the analysis the theoretical stability conditions and all the available experimental results. Since the Higgs precision data strongly prefers the SM-like Higgs boson for large  $t_\beta$ , we assumed the Higgs alignment. Two possible scenarios are studied, the normal scenario where the lighter  $CP$ -even  $h$  becomes  $h_{\text{SM}}$  and the inverted scenario where the heavier  $CP$ -even  $H$  is  $h_{\text{SM}}$ . The model has five physical parameters,  $m_{\varphi^0}$ ,  $M_A$ ,  $M_{H^\pm}$ ,  $M^2 (= m_{12}^2/s_\beta/c_\beta)$ , and  $t_\beta$ , where  $\varphi^0 = H(h)$  in the normal (inverted) scenario.

The various conditions cause a chain reaction of constraining the model parameters. First, the large and positive  $\Delta a_\mu^{\text{obs}}$  requires huge  $t_\beta$  above  $\gtrsim 100$ , which makes the  $\tau^\pm$  loop of the two-loop Barr-Zee diagram dominant. The contribution of  $\varphi^0$ , the new  $CP$ -even scalar boson, is negative. Decoupling  $\varphi^0$  to suppress the negative contribution conflicts the theoretical stability. The most sensitive one is the Higgs quartic coupling  $\lambda_1$ , which has a term proportional to  $t_\beta^2$ . For  $t_\beta \gtrsim 100$ , the perturbativity and the unitarity are easily broken unless the  $t_\beta^2$  term of  $\lambda_1$  vanishes. We cannot avoid  $m_{\varphi^0}^2 \approx M^2$ , which subsequently demands  $M_A \simeq M_{H^\pm} \simeq M \approx m_{\varphi^0}$ . As decoupling  $\varphi^0$  and  $H^\pm$  becomes unworkable, sizable negative contributions of  $\varphi^0$  is inevitable, which increases  $t_\beta$  and lowers  $M_A$  to explain  $\Delta a_\mu^{\text{obs}}$ . Finally, we found that the direct search bounds at the LEP and LHC exclude a large portion of the parameter space. In the normal scenario,  $h_{\text{SM}} \rightarrow AA$  at the LHC is the smoking-gun signal, eliminating the cases of  $M_A < m_{125}/2$ . In the inverted scenario, the most crucial one is the LEP search for  $e^+e^- \rightarrow Z^* \rightarrow Ah$ .

For the full picture of the model phenomenology, we summarize the allowed parameters as follows:

- In the normal scenario
  - $t_\beta \gtrsim 90$  and  $M_A \in [m_{125}/2, 145]$  GeV;
  - $M_H \in [130, 245]$  GeV and  $M_{H^\pm} \in [95, 285]$  GeV.
- In the inverted scenario
  - $t_\beta \gtrsim 120$  and  $M_A \in [70, 105]$  GeV;
  - $M_H \in [100, 120]$  GeV and  $M_{H^\pm} \in [95, 185]$  GeV;
  - $M_A + M_h \gtrsim 190$  GeV due to the LEP process of  $e^+e^- \rightarrow Z^* \rightarrow Zh$ .

For the finally surviving parameter points, we calculate the electron anomalous magnetic moment. The predicted values are consistent with the observation,  $\Delta a_e$  using the fine structure constant  $\alpha$  from  $^{133}\text{Cs}$  at  $3\sigma$ , and  $\Delta a_e$  using  $\alpha$  from  $^{87}\text{Rb}$  at  $2\sigma$ . For the LHC searches, we proposed two processes of the hadro-phobic new scalar bosons,  $pp \rightarrow A\varphi^0 \rightarrow 4\tau$  and  $pp \rightarrow H^+H^- \rightarrow \tau\nu\tau\nu$ . Both depend on the gauge couplings, almost irrespective of  $t_\beta$ . We found that particularly  $pp \rightarrow A\varphi^0 \rightarrow 4\tau$  has high potential to probe the model. The

total cross section at the 14 TeV LHC lies around  $25 \sim 260$  fb in the normal scenario and  $180 \sim 300$  fb in the inverted scenario.

The new measurement of the muon  $g - 2$  supports the long-lasting deviation from the SM prediction, pointing to the advent of a new physics era. As we have shown that the existing experimental data significantly constrain the parameter space of the Type-X 2HDM where the observed  $\Delta a_\mu$  is explained, the future high energy collider data shall greatly help us to reveal the nature of new physics.

## Acknowledgments

We would like to thank Kingman Cheung and Chih-Ting Lu for useful discussions. This work is supported by the National Research Foundation of Korea, Grant No. NRF-2019R1A2C1009419.

## References

- [1] MUON G-2 collaboration, B. Abi et al., *Measurement of the Positive Muon Anomalous Magnetic Moment to 0.46 ppm*, [Phys. Rev. Lett.](#) **126** (2021) 141801, [[2104.03281](#)].
- [2] MUON G-2 collaboration, T. Albahri et al., *Measurement of the anomalous precession frequency of the muon in the Fermilab Muon  $g - 2$  Experiment*, [Phys. Rev. D](#) **103** (2021) 072002, [[2104.03247](#)].
- [3] MUON G-2 collaboration, G. W. Bennett et al., *Final Report of the Muon E821 Anomalous Magnetic Moment Measurement at BNL*, [Phys. Rev. D](#) **73** (2006) 072003, [[hep-ex/0602035](#)].
- [4] T. Aoyama, M. Hayakawa, T. Kinoshita and M. Nio, *Complete Tenth-Order QED Contribution to the Muon  $g-2$* , [Phys. Rev. Lett.](#) **109** (2012) 111808, [[1205.5370](#)].
- [5] A. Czarnecki, W. J. Marciano and A. Vainshtein, *Refinements in electroweak contributions to the muon anomalous magnetic moment*, [Phys. Rev. D](#) **67** (2003) 073006, [[hep-ph/0212229](#)].
- [6] C. Gnendiger, D. Stöckinger and H. Stöckinger-Kim, *The electroweak contributions to  $(g - 2)_\mu$  after the Higgs boson mass measurement*, [Phys. Rev. D](#) **88** (2013) 053005, [[1306.5546](#)].
- [7] A. Kurz, T. Liu, P. Marquard and M. Steinhauser, *Hadronic contribution to the muon anomalous magnetic moment to next-to-next-to-leading order*, [Phys. Lett. B](#) **734** (2014) 144–147, [[1403.6400](#)].
- [8] M. Davier, A. Hoecker, B. Malaescu and Z. Zhang, *Reevaluation of the hadronic vacuum polarisation contributions to the Standard Model predictions of the muon  $g - 2$  and  $\alpha(m_Z^2)$  using newest hadronic cross-section data*, [Eur. Phys. J. C](#) **77** (2017) 827, [[1706.09436](#)].
- [9] G. Colangelo, M. Hoferichter and P. Stoffer, *Two-pion contribution to hadronic vacuum polarization*, [JHEP](#) **02** (2019) 006, [[1810.00007](#)].
- [10] A. Keshavarzi, D. Nomura and T. Teubner, *Muon  $g - 2$  and  $\alpha(M_Z^2)$ : a new data-based analysis*, [Phys. Rev. D](#) **97** (2018) 114025, [[1802.02995](#)].

- [11] A. Keshavarzi, D. Nomura and T. Teubner,  $g - 2$  of charged leptons,  $\alpha(M_Z^2)$ , and the hyperfine splitting of muonium, [Phys. Rev. D](#) **101** (2020) 014029, [[1911.00367](#)].
- [12] M. Davier, A. Hoecker, B. Malaescu and Z. Zhang, A new evaluation of the hadronic vacuum polarisation contributions to the muon anomalous magnetic moment and to  $\alpha(m_Z^2)$ , [Eur. Phys. J. C](#) **80** (2020) 241, [[1908.00921](#)].
- [13] B.-L. Hoid, M. Hoferichter and B. Kubis, Hadronic vacuum polarization and vector-meson resonance parameters from  $e^+e^- \rightarrow \pi^0\gamma$ , [Eur. Phys. J. C](#) **80** (2020) 988, [[2007.12696](#)].
- [14] G. Colangelo, M. Hoferichter and P. Stoffer, Constraints on the two-pion contribution to hadronic vacuum polarization, [Phys. Lett. B](#) **814** (2021) 136073, [[2010.07943](#)].
- [15] K. Melnikov and A. Vainshtein, Hadronic light-by-light scattering contribution to the muon anomalous magnetic moment revisited, [Phys. Rev. D](#) **70** (2004) 113006, [[hep-ph/0312226](#)].
- [16] G. Colangelo, M. Hoferichter, B. Kubis, M. Procura and P. Stoffer, Towards a data-driven analysis of hadronic light-by-light scattering, [Phys. Lett. B](#) **738** (2014) 6–12, [[1408.2517](#)].
- [17] G. Colangelo, M. Hoferichter, A. Nyffeler, M. Passera and P. Stoffer, Remarks on higher-order hadronic corrections to the muon  $g-2$ , [Phys. Lett. B](#) **735** (2014) 90–91, [[1403.7512](#)].
- [18] G. Colangelo, M. Hoferichter, M. Procura and P. Stoffer, Dispersion relation for hadronic light-by-light scattering: theoretical foundations, [JHEP](#) **09** (2015) 074, [[1506.01386](#)].
- [19] G. Colangelo, M. Hoferichter, M. Procura and P. Stoffer, Dispersion relation for hadronic light-by-light scattering: two-pion contributions, [JHEP](#) **04** (2017) 161, [[1702.07347](#)].
- [20] P. Masjuan and P. Sanchez-Puertas, Pseudoscalar-pole contribution to the  $(g_\mu - 2)$ : a rational approach, [Phys. Rev. D](#) **95** (2017) 054026, [[1701.05829](#)].
- [21] G. Colangelo, M. Hoferichter, M. Procura and P. Stoffer, Rescattering effects in the hadronic-light-by-light contribution to the anomalous magnetic moment of the muon, [Phys. Rev. Lett.](#) **118** (2017) 232001, [[1701.06554](#)].
- [22] M. Hoferichter, B.-L. Hoid, B. Kubis, S. Leupold and S. P. Schneider, Pion-pole contribution to hadronic light-by-light scattering in the anomalous magnetic moment of the muon, [Phys. Rev. Lett.](#) **121** (2018) 112002, [[1805.01471](#)].
- [23] M. Hoferichter, B.-L. Hoid, B. Kubis, S. Leupold and S. P. Schneider, Dispersion relation for hadronic light-by-light scattering: pion pole, [JHEP](#) **10** (2018) 141, [[1808.04823](#)].
- [24] G. Colangelo, F. Hagelstein, M. Hoferichter, L. Laub and P. Stoffer, Short-distance constraints on hadronic light-by-light scattering in the anomalous magnetic moment of the muon, [Phys. Rev. D](#) **101** (2020) 051501, [[1910.11881](#)].
- [25] J. Bijnens, N. Hermansson-Truedsson and A. Rodríguez-Sánchez, Short-distance constraints for the HLbL contribution to the muon anomalous magnetic moment, [Phys. Lett. B](#) **798** (2019) 134994, [[1908.03331](#)].
- [26] T. Blum, N. Christ, M. Hayakawa, T. Izubuchi, L. Jin, C. Jung et al., Hadronic Light-by-Light Scattering Contribution to the Muon Anomalous Magnetic Moment from Lattice QCD, [Phys. Rev. Lett.](#) **124** (2020) 132002, [[1911.08123](#)].
- [27] J. Bijnens, N. Hermansson-Truedsson, L. Laub and A. Rodríguez-Sánchez, Short-distance HLbL contributions to the muon anomalous magnetic moment beyond perturbation theory, [JHEP](#) **10** (2020) 203, [[2008.13487](#)].

- [28] S. Borsanyi et al., *Leading hadronic contribution to the muon  $g - 2$  magnetic moment from lattice QCD*, [2002.12347](#).
- [29] C. Lehner and A. S. Meyer, *Consistency of hadronic vacuum polarization between lattice QCD and the  $R$ -ratio*, [Phys. Rev. D](#) **101** (2020) 074515, [[2003.04177](#)].
- [30] A. Crivellin, M. Hoferichter, C. A. Manzari and M. Montull, *Hadronic Vacuum Polarization:  $(g - 2)_\mu$  versus Global Electroweak Fits*, [Phys. Rev. Lett.](#) **125** (2020) 091801, [[2003.04886](#)].
- [31] A. Keshavarzi, W. J. Marciano, M. Passera and A. Sirlin, *Muon  $g - 2$  and  $\Delta\alpha$  connection*, [Phys. Rev. D](#) **102** (2020) 033002, [[2006.12666](#)].
- [32] B. Malaescu and M. Schott, *Impact of correlations between  $a_\mu$  and  $\alpha_{QED}$  on the EW fit*, [Eur. Phys. J. C](#) **81** (2021) 46, [[2008.08107](#)].
- [33] A. Czarnecki and W. J. Marciano, *The Muon anomalous magnetic moment: A Harbinger for 'new physics'*, [Phys. Rev. D](#) **64** (2001) 013014, [[hep-ph/0102122](#)].
- [34] H. Baer, V. Barger and H. Serce, *Anomalous muon magnetic moment, supersymmetry, naturalness, LHC search limits and the landscape*, [2104.07597](#).
- [35] A. Aboubrahim, M. Klasen and P. Nath, *What Fermilab  $(g - 2)_\mu$  experiment tells us about discovering SUSY at HL-LHC and HE-LHC*, [2104.03839](#).
- [36] J. Cao, J. Lian, Y. Pan, D. Zhang and P. Zhu, *Improved  $(g - 2)_\mu$  Measurement and Singlino dark matter in the general NMSSM*, [2104.03284](#).
- [37] F. Wang, L. Wu, Y. Xiao, J. M. Yang and Y. Zhang, *GUT-scale constrained SUSY in light of E989 muon  $g-2$  measurement*, [2104.03262](#).
- [38] M. Van Beekveld, W. Beenakker, M. Schutten and J. De Wit, *Dark matter, fine-tuning and  $(g - 2)_\mu$  in the pMSSM*, [2104.03245](#).
- [39] M. Abdughani, Y.-Z. Fan, L. Feng, Y.-L. Sming Tsai, L. Wu and Q. Yuan, *A common origin of muon  $g-2$  anomaly, Galaxy Center GeV excess and AMS-02 anti-proton excess in the NMSSM*, [2104.03274](#).
- [40] S. Baum, M. Carena, N. R. Shah and C. E. M. Wagner, *The Tiny  $(g-2)$  Muon Wobble from Small- $\mu$  Supersymmetry*, [2104.03302](#).
- [41] W. Ahmed, I. Khan, J. Li, T. Li, S. Raza and W. Zhang, *The Natural Explanation of the Muon Anomalous Magnetic Moment via the Electroweak Supersymmetry from the GmSUGRA in the MSSM*, [2104.03491](#).
- [42] H.-B. Zhang, C.-X. Liu, J.-L. Yang and T.-F. Feng, *Muon anomalous magnetic dipole moment in the  $\mu\nu$ SMS*, [2104.03489](#).
- [43] M. Chakraborti, L. Roszkowski and S. Trojanowski, *GUT-constrained supersymmetry and dark matter in light of the new  $(g - 2)_\mu$  determination*, [2104.04458](#).
- [44] P. Athron, C. Balázs, D. H. Jacob, W. Kotlarski, D. Stöckinger and H. Stöckinger-Kim, *New physics explanations of  $a_\mu$  in light of the FNAL muon  $g - 2$  measurement*, [2104.03691](#).
- [45] W. Yin, *Muon  $g - 2$  Anomaly in Anomaly Mediation*, [2104.03259](#).
- [46] A. J. Buras, A. Crivellin, F. Kirk, C. A. Manzari and M. Montull, *Global Analysis of Leptophilic  $Z'$  Bosons*, [2104.07680](#).

- [47] E. J. Chun and T. Mondal, *Leptophilic bosons and muon  $g-2$  at lepton colliders*, [2104.03701](#).
- [48] J. Liu, C. E. M. Wagner and X.-P. Wang, *A light complex scalar for the electron and muon anomalous magnetic moments*, [JHEP 03 \(2019\) 008](#), [[1810.11028](#)].
- [49] A. E. Cárcamo Hernández, S. Kovalenko, M. Maniatis and I. Schmidt, *Fermion mass hierarchy and  $g-2$  anomalies in an extended 3HDM Model*, [2104.07047](#).
- [50] K. Ban, Y. Jho, Y. Kwon, S. C. Park, S. Park and P.-Y. Tseng, *A comprehensive study of vector leptoquark on the  $B$ -meson and Muon  $g-2$  anomalies*, [2104.06656](#).
- [51] M. Du, J. Liang, Z. Liu and V. Q. Tran, *A vector leptoquark interpretation of the muon  $g - 2$  and  $B$  anomalies*, [2104.05685](#).
- [52] D. Borah, M. Dutta, S. Mahapatra and N. Sahu, *Muon  $(g - 2)$  and XENON1T Excess with Boosted Dark Matter in  $L_\mu - L_\tau$  Model*, [2104.05656](#).
- [53] L. Zu, X. Pan, L. Feng, Q. Yuan and Y.-Z. Fan, *Constraining  $U(1)_{L_\mu - L_\tau}$  charged dark matter model for muon  $g - 2$  anomaly with AMS-02 electron and positron data*, [2104.03340](#).
- [54] J.-L. Yang, H.-B. Zhang, C.-X. Liu, X.-X. Dong and T.-F. Feng, *Muon  $(g - 2)$  in the  $B$ -LSSM*, [2104.03542](#).
- [55] A. Greljo, P. Stangl and A. E. Thomsen, *A Model of Muon Anomalies*, [2103.13991](#).
- [56] B. Zhu and X. Liu, *Probing light dark matter with scalar mediator: muon  $(g - 2)$  deviation, the proton radius puzzle*, [2104.03238](#).
- [57] P. Escribano, J. Terol-Calvo and A. Vicente,  *$(g - 2)_{e,\mu}$  in an extended inverse type-III seesaw*, [2104.03705](#).
- [58] G. Arcadi, L. Calibbi, M. Fedele and F. Mescia, *Muon  $g - 2$  and  $B$ -anomalies from Dark Matter*, [2104.03228](#).
- [59] A. Crivellin and M. Hoferichter, *Consequences of chirally enhanced explanations of  $(g - 2)_\mu$  for  $h \rightarrow \mu\mu$  and  $Z \rightarrow \mu\mu$* , [2104.03202](#).
- [60] M. A. Buen-Abad, J. Fan, M. Reece and C. Sun, *Challenges for an axion explanation of the muon  $g - 2$  measurement*, [2104.03267](#).
- [61] S.-F. Ge, X.-D. Ma and P. Pasquini, *Probing the Dark Axion Portal with Muon Anomalous Magnetic Moment*, [2104.03276](#).
- [62] P. M. Ferreira, B. L. Gonçalves, F. R. Joaquim and M. Sher,  *$(g - 2)_\mu$  in the 2HDM and slightly beyond – an updated view*, [2104.03367](#).
- [63] X.-F. Han, T. Li, H.-X. Wang, L. Wang and Y. Zhang, *Lepton-specific inert two-Higgs-doublet model confronted with the new results for muon and electron  $g-2$  anomalies and multi-lepton searches at the LHC*, [2104.03227](#).
- [64] C.-H. Chen, C.-W. Chiang and T. Nomura, *Muon  $g - 2$  in two-Higgs-doublet model with type-II seesaw mechanism*, [2104.03275](#).
- [65] N. Ghosh and J. Lahiri, *Revisiting a generalized two-Higgs-doublet model in light of the muon anomaly and lepton flavor violating decays at the HL-LHC*, [Phys. Rev. D 103 \(2021\) 055009](#), [[2010.03590](#)].
- [66] N. Ghosh and J. Lahiri, *Generalized 2HDM with wrong-sign lepton Yukawa coupling, in light of  $g_\mu - 2$  and lepton flavor violation at the future LHC*, [2103.10632](#).

- [67] S.-P. Li, X.-Q. Li, Y.-Y. Li, Y.-D. Yang and X. Zhang, *Power-aligned 2HDM: a correlative perspective on  $(g - 2)_{e,\mu}$* , [JHEP](#) **01** (2021) 034, [[2010.02799](#)].
- [68] S. Jana, V. P. K. and S. Saad, *Resolving electron and muon  $g - 2$  within the 2HDM*, [Phys. Rev. D](#) **101** (2020) 115037, [[2003.03386](#)].
- [69] S. Jana, P. K. Vishnu, W. Rodejohann and S. Saad, *Dark matter assisted lepton anomalous magnetic moments and neutrino masses*, [Phys. Rev. D](#) **102** (2020) 075003, [[2008.02377](#)].
- [70] D. Anselmi, K. Kannike, C. Marzo, L. Marzola, A. Melis, K. Mürsepp et al., *A fake doublet solution to the muon anomalous magnetic moment*, [2104.03249](#).
- [71] D. Sabatta, A. S. Cornell, A. Goyal, M. Kumar, B. Mellado and X. Ruan, *Connecting muon anomalous magnetic moment and multi-lepton anomalies at LHC*, [Chin. Phys. C](#) **44** (2020) 063103, [[1909.03969](#)].
- [72] K. Schmidt-Hoberg, F. Staub and M. W. Winkler, *Constraints on light mediators: confronting dark matter searches with B physics*, [Phys. Lett. B](#) **727** (2013) 506–510, [[1310.6752](#)].
- [73] A. Broggio, E. J. Chun, M. Passera, K. M. Patel and S. K. Vempati, *Limiting two-Higgs-doublet models*, [JHEP](#) **11** (2014) 058, [[1409.3199](#)].
- [74] L. Wang and X.-F. Han, *A light pseudoscalar of 2HDM confronted with muon  $g-2$  and experimental constraints*, [JHEP](#) **05** (2015) 039, [[1412.4874](#)].
- [75] T. Abe, R. Sato and K. Yagyu, *Lepton-specific two Higgs doublet model as a solution of muon  $g - 2$  anomaly*, [JHEP](#) **07** (2015) 064, [[1504.07059](#)].
- [76] L. Wang, J. M. Yang, M. Zhang and Y. Zhang, *Revisiting lepton-specific 2HDM in light of muon  $g - 2$  anomaly*, [Phys. Lett. B](#) **788** (2019) 519–529, [[1809.05857](#)].
- [77] J. Cao, P. Wan, L. Wu and J. M. Yang, *Lepton-Specific Two-Higgs Doublet Model: Experimental Constraints and Implication on Higgs Phenomenology*, [Phys. Rev. D](#) **80** (2009) 071701, [[0909.5148](#)].
- [78] G. C. Branco, P. M. Ferreira, L. Lavoura, M. N. Rebelo, M. Sher and J. P. Silva, *Theory and phenomenology of two-Higgs-doublet models*, [Phys. Rept.](#) **516** (2012) 1–102, [[1106.0034](#)].
- [79] S. L. Glashow and S. Weinberg, *Natural Conservation Laws for Neutral Currents*, [Phys. Rev.](#) **D15** (1977) 1958.
- [80] E. A. Paschos, *Diagonal Neutral Currents*, [Phys. Rev.](#) **D15** (1977) 1966.
- [81] J. Song and Y. W. Yoon,  *$W\gamma$  decay of the elusive charged Higgs boson in the two-Higgs-doublet model with vectorlike fermions*, [Phys. Rev.](#) **D100** (2019) 055006, [[1904.06521](#)].
- [82] M. Aoki, S. Kanemura, K. Tsumura and K. Yagyu, *Models of Yukawa interaction in the two Higgs doublet model, and their collider phenomenology*, [Phys. Rev.](#) **D80** (2009) 015017, [[0902.4665](#)].
- [83] ATLAS collaboration, *A combination of measurements of Higgs boson production and decay using up to  $139 \text{ fb}^{-1}$  of proton–proton collision data at  $\sqrt{s} = 13 \text{ TeV}$  collected with the ATLAS experiment*, .
- [84] M. Carena, I. Low, N. R. Shah and C. E. M. Wagner, *Impersonating the Standard Model Higgs Boson: Alignment without Decoupling*, [JHEP](#) **04** (2014) 015, [[1310.2248](#)].

- [85] A. Celis, V. Ilisie and A. Pich, *LHC constraints on two-Higgs doublet models*, [JHEP](#) **07** (2013) 053, [[1302.4022](#)].
- [86] J. Bernon, J. F. Gunion, H. E. Haber, Y. Jiang and S. Kraml, *Scrutinizing the alignment limit in two-Higgs-doublet models:  $m_h=125$  GeV*, [Phys. Rev. D](#) **92** (2015) 075004, [[1507.00933](#)].
- [87] S. Chang, S. K. Kang, J.-P. Lee and J. Song, *Higgs potential and hidden light Higgs scenario in two Higgs doublet models*, [Phys. Rev. D](#) **92** (2015) 075023, [[1507.03618](#)].
- [88] D. Das and I. Saha, *Search for a stable alignment limit in two-Higgs-doublet models*, [Phys. Rev. D](#) **91** (2015) 095024, [[1503.02135](#)].
- [89] J. Bernon, J. F. Gunion, H. E. Haber, Y. Jiang and S. Kraml, *Scrutinizing the alignment limit in two-Higgs-doublet models. II.  $m_H=125$  GeV*, [Phys. Rev. D](#) **93** (2016) 035027, [[1511.03682](#)].
- [90] S. Kanemura, Y. Okada, H. Taniguchi and K. Tsumura, *Indirect bounds on heavy scalar masses of the two-Higgs-doublet model in light of recent Higgs boson searches*, [Phys. Lett. B](#) **704** (2011) 303–307, [[1108.3297](#)].
- [91] ATLAS collaboration, G. Aad et al., *Combined measurements of Higgs boson production and decay using up to  $80 \text{ fb}^{-1}$  of proton-proton collision data at  $\sqrt{s} = 13$  TeV collected with the ATLAS experiment*, [Phys. Rev. D](#) **101** (2020) 012002, [[1909.02845](#)].
- [92] S. M. Barr and A. Zee, *Electric Dipole Moment of the Electron and of the Neutron*, [Phys. Rev. Lett.](#) **65** (1990) 21–24.
- [93] V. Ilisie, *New Barr-Zee contributions to  $(\mathbf{g} - \mathbf{2})_\mu$  in two-Higgs-doublet models*, [JHEP](#) **04** (2015) 077, [[1502.04199](#)].
- [94] E. J. Chun and J. Kim, *Leptonic Precision Test of Leptophilic Two-Higgs-Doublet Model*, [JHEP](#) **07** (2016) 110, [[1605.06298](#)].
- [95] A. Barroso, P. M. Ferreira, I. P. Ivanov and R. Santos, *Metastability bounds on the two Higgs doublet model*, [JHEP](#) **06** (2013) 045, [[1303.5098](#)].
- [96] I. P. Ivanov, *Minkowski space structure of the Higgs potential in 2HDM*, [Phys. Rev. D](#) **75** (2007) 035001, [[hep-ph/0609018](#)].
- [97] A. Arhrib, *Unitarity constraints on scalar parameters of the standard and two Higgs doublets model*, in [Workshop on Noncommutative Geometry, Superstrings and Particle Physics](#), 12, 2000. [hep-ph/0012353](#).
- [98] PARTICLE DATA GROUP collaboration, P. A. Zyla et al., *Review of Particle Physics*, [PTEP](#) **2020** (2020) 083C01.
- [99] H.-J. He, N. Polonsky and S.-f. Su, *Extra families, Higgs spectrum and oblique corrections*, [Phys. Rev. D](#) **64** (2001) 053004, [[hep-ph/0102144](#)].
- [100] W. Grimus, L. Lavoura, O. M. Ogreid and P. Osland, *The Oblique parameters in multi-Higgs-doublet models*, [Nucl. Phys. B](#) **801** (2008) 81–96, [[0802.4353](#)].
- [101] P. Bechtle, S. Heinemeyer, O. Stål, T. Stefaniak and G. Weiglein, *HiggsSignals: Confronting arbitrary Higgs sectors with measurements at the Tevatron and the LHC*, [Eur. Phys. J. C](#) **74** (2014) 2711, [[1305.1933](#)].
- [102] P. Bechtle, S. Heinemeyer, T. Klingl, T. Stefaniak, G. Weiglein and J. Wittbrodt,

*HiggsSignals-2: Probing new physics with precision Higgs measurements in the LHC 13 TeV era*, [Eur. Phys. J. C](#) **81** (2021) 145, [[2012.09197](#)].

- [103] P. Bechtle, D. Dercks, S. Heinemeyer, T. Klingl, T. Stefaniak, G. Weiglein et al., *HiggsBounds-5: Testing Higgs Sectors in the LHC 13 TeV Era*, [Eur. Phys. J. C](#) **80** (2020) 1211, [[2006.06007](#)].
- [104] ALEPH, DELPHI, L3, OPAL, LEP WORKING GROUP FOR HIGGS BOSON SEARCHES collaboration, S. Schael et al., *Search for neutral MSSM Higgs bosons at LEP*, [Eur. Phys. J. C](#) **47** (2006) 547–587, [[hep-ex/0602042](#)].
- [105] ATLAS collaboration, M. Aaboud et al., *Search for Higgs boson decays into a pair of light bosons in the  $b\bar{b}\mu\mu$  final state in  $pp$  collision at  $\sqrt{s} = 13$  TeV with the ATLAS detector*, [Phys. Lett. B](#) **790** (2019) 1–21, [[1807.00539](#)].
- [106] ATLAS collaboration, M. Aaboud et al., *Search for the Higgs boson produced in association with a vector boson and decaying into two spin-zero particles in the  $H \rightarrow aa \rightarrow 4b$  channel in  $pp$  collisions at  $\sqrt{s} = 13$  TeV with the ATLAS detector*, [JHEP](#) **10** (2018) 031, [[1806.07355](#)].
- [107] CMS collaboration, A. M. Sirunyan et al., *Search for an exotic decay of the Higgs boson to a pair of light pseudoscalars in the final state of two muons and two  $\tau$  leptons in proton-proton collisions at  $\sqrt{s} = 13$  TeV*, [JHEP](#) **11** (2018) 018, [[1805.04865](#)].
- [108] CMS collaboration, A. M. Sirunyan et al., *Search for an exotic decay of the Higgs boson to a pair of light pseudoscalars in the final state with two muons and two  $b$  quarks in  $pp$  collisions at 13 TeV*, [Phys. Lett. B](#) **795** (2019) 398–423, [[1812.06359](#)].
- [109] CMS collaboration, A. M. Sirunyan et al., *Search for an exotic decay of the Higgs boson to a pair of light pseudoscalars in the final state with two  $b$  quarks and two  $\tau$  leptons in proton-proton collisions at  $\sqrt{s} = 13$  TeV*, [Phys. Lett. B](#) **785** (2018) 462, [[1805.10191](#)].
- [110] CMS collaboration, A. M. Sirunyan et al., *Search for light pseudoscalar boson pairs produced from decays of the 125 GeV Higgs boson in final states with two muons and two nearby tracks in  $pp$  collisions at  $\sqrt{s} = 13$  TeV*, [Phys. Lett. B](#) **800** (2020) 135087, [[1907.07235](#)].
- [111] ATLAS collaboration, M. Aaboud et al., *Combination of searches for heavy resonances decaying into bosonic and leptonic final states using  $36 \text{ fb}^{-1}$  of proton-proton collision data at  $\sqrt{s} = 13$  TeV with the ATLAS detector*, [Phys. Rev. D](#) **98** (2018) 052008, [[1808.02380](#)].
- [112] CMS collaboration, A. M. Sirunyan et al., *Search for a new scalar resonance decaying to a pair of  $Z$  bosons in proton-proton collisions at  $\sqrt{s} = 13$  TeV*, [JHEP](#) **06** (2018) 127, [[1804.01939](#)].
- [113] CMS collaboration, A. M. Sirunyan et al., *Search for a heavy Higgs boson decaying to a pair of  $W$  bosons in proton-proton collisions at  $\sqrt{s} = 13$  TeV*, [JHEP](#) **03** (2020) 034, [[1912.01594](#)].
- [114] ATLAS collaboration, M. Aaboud et al., *Search for Higgs boson pair production in the  $\gamma\gamma WW^*$  channel using  $pp$  collision data recorded at  $\sqrt{s} = 13$  TeV with the ATLAS detector*, [Eur. Phys. J. C](#) **78** (2018) 1007, [[1807.08567](#)].
- [115] ATLAS collaboration, M. Aaboud et al., *Search for pair production of Higgs bosons in the  $b\bar{b}b\bar{b}$  final state using proton-proton collisions at  $\sqrt{s} = 13$  TeV with the ATLAS detector*, [JHEP](#) **01** (2019) 030, [[1804.06174](#)].

- [116] ATLAS collaboration, M. Aaboud et al., *Search for Higgs boson pair production in the  $WW^{(*)}WW^{(*)}$  decay channel using ATLAS data recorded at  $\sqrt{s} = 13$  TeV*, [JHEP](#) **05** (2019) 124, [[1811.11028](#)].
- [117] ATLAS collaboration, M. Aaboud et al., *Search for resonant and non-resonant Higgs boson pair production in the  $b\bar{b}\tau^+\tau^-$  decay channel in  $pp$  collisions at  $\sqrt{s} = 13$  TeV with the ATLAS detector*, [Phys. Rev. Lett.](#) **121** (2018) 191801, [[1808.00336](#)].
- [118] ATLAS collaboration, G. Aad et al., *Combination of searches for Higgs boson pairs in  $pp$  collisions at  $\sqrt{s} = 13$  TeV with the ATLAS detector*, [Phys. Lett. B](#) **800** (2020) 135103, [[1906.02025](#)].
- [119] ATLAS collaboration, G. Aad et al., *Search for the  $HH \rightarrow b\bar{b}b\bar{b}$  process via vector-boson fusion production using proton-proton collisions at  $\sqrt{s} = 13$  TeV with the ATLAS detector*, [JHEP](#) **07** (2020) 108, [[2001.05178](#)].
- [120] CMS collaboration, A. M. Sirunyan et al., *Combination of searches for Higgs boson pair production in proton-proton collisions at  $\sqrt{s} = 13$  TeV*, [Phys. Rev. Lett.](#) **122** (2019) 121803, [[1811.09689](#)].
- [121] ATLAS collaboration, M. Aaboud et al., *Search for new phenomena in high-mass diphoton final states using  $37\text{ fb}^{-1}$  of proton-proton collisions collected at  $\sqrt{s} = 13$  TeV with the ATLAS detector*, [Phys. Lett. B](#) **775** (2017) 105–125, [[1707.04147](#)].
- [122] CMS collaboration, A. M. Sirunyan et al., *Search for a standard model-like Higgs boson in the mass range between 70 and 110 GeV in the diphoton final state in proton-proton collisions at  $\sqrt{s} = 8$  and 13 TeV*, [Phys. Lett. B](#) **793** (2019) 320–347, [[1811.08459](#)].
- [123] ATLAS collaboration, G. Aad et al., *Search for heavy Higgs bosons decaying into two tau leptons with the ATLAS detector using  $pp$  collisions at  $\sqrt{s} = 13$  TeV*, [Phys. Rev. Lett.](#) **125** (2020) 051801, [[2002.12223](#)].
- [124] CMS collaboration, A. M. Sirunyan et al., *Search for additional neutral MSSM Higgs bosons in the  $\tau\tau$  final state in proton-proton collisions at  $\sqrt{s} = 13$  TeV*, [JHEP](#) **09** (2018) 007, [[1803.06553](#)].
- [125] ATLAS collaboration, G. Aad et al., *Search for high-mass dilepton resonances using  $139\text{ fb}^{-1}$  of  $pp$  collision data collected at  $\sqrt{s} = 13$  TeV with the ATLAS detector*, [Phys. Lett. B](#) **796** (2019) 68–87, [[1903.06248](#)].
- [126] ATLAS collaboration, M. Aaboud et al., *Search for scalar resonances decaying into  $\mu^+\mu^-$  in events with and without  $b$ -tagged jets produced in proton-proton collisions at  $\sqrt{s} = 13$  TeV with the ATLAS detector*, [JHEP](#) **07** (2019) 117, [[1901.08144](#)].
- [127] CMS collaboration, A. M. Sirunyan et al., *Search for MSSM Higgs bosons decaying to  $\mu + \mu -$  in proton-proton collisions at  $s=13\text{TeV}$* , [Phys. Lett. B](#) **798** (2019) 134992, [[1907.03152](#)].
- [128] ATLAS collaboration, G. Aad et al., *Search for heavy neutral Higgs bosons produced in association with  $b$ -quarks and decaying into  $b$ -quarks at  $\sqrt{s} = 13$  TeV with the ATLAS detector*, [Phys. Rev. D](#) **102** (2020) 032004, [[1907.02749](#)].
- [129] CMS collaboration, A. M. Sirunyan et al., *Search for low-mass resonances decaying into bottom quark-antiquark pairs in proton-proton collisions at  $\sqrt{s} = 13$  TeV*, [Phys. Rev. D](#) **99** (2019) 012005, [[1810.11822](#)].
- [130] CMS collaboration, A. M. Sirunyan et al., *Search for beyond the standard model Higgs*

- bosons decaying into a  $b\bar{b}$  pair in pp collisions at  $\sqrt{s} = 13$  TeV*, [JHEP](#) **08** (2018) 113, [[1805.12191](#)].
- [131] CMS collaboration, A. M. Sirunyan et al., *Search for heavy Higgs bosons decaying to a top quark pair in proton-proton collisions at  $\sqrt{s} = 13$  TeV*, [JHEP](#) **04** (2020) 171, [[1908.01115](#)].
- [132] ATLAS collaboration, G. Aad et al., *Search for a CP-odd Higgs boson decaying to Zh in pp collisions at  $\sqrt{s} = 8$  TeV with the ATLAS detector*, [Phys. Lett. B](#) **744** (2015) 163–183, [[1502.04478](#)].
- [133] CMS collaboration, A. M. Sirunyan et al., *Search for a heavy pseudoscalar boson decaying to a Z and a Higgs boson at  $\sqrt{s} = 13$  TeV*, [Eur. Phys. J. C](#) **79** (2019) 564, [[1903.00941](#)].
- [134] ATLAS collaboration, M. Aaboud et al., *Search for a heavy Higgs boson decaying into a Z boson and another heavy Higgs boson in the  $\ell b\bar{b}$  final state in pp collisions at  $\sqrt{s} = 13$  TeV with the ATLAS detector*, [Phys. Lett. B](#) **783** (2018) 392–414, [[1804.01126](#)].
- [135] CMS collaboration, A. M. Sirunyan et al., *Search for new neutral Higgs bosons through the  $H \rightarrow ZA \rightarrow \ell^+ \ell^- b\bar{b}$  process in pp collisions at  $\sqrt{s} = 13$  TeV*, [JHEP](#) **03** (2020) 055, [[1911.03781](#)].
- [136] ATLAS collaboration, M. Aaboud et al., *Search for charged Higgs bosons decaying into top and bottom quarks at  $\sqrt{s} = 13$  TeV with the ATLAS detector*, [JHEP](#) **11** (2018) 085, [[1808.03599](#)].
- [137] CMS collaboration, A. M. Sirunyan et al., *Search for charged Higgs bosons decaying into a top and a bottom quark in the all-jet final state of pp collisions at  $\sqrt{s} = 13$  TeV*, [JHEP](#) **07** (2020) 126, [[2001.07763](#)].
- [138] ATLAS collaboration, M. Aaboud et al., *Search for charged Higgs bosons decaying via  $H^\pm \rightarrow \tau^\pm \nu_\tau$  in the  $\tau$ +jets and  $\tau$ +lepton final states with  $36 \text{ fb}^{-1}$  of pp collision data recorded at  $\sqrt{s} = 13$  TeV with the ATLAS experiment*, [JHEP](#) **09** (2018) 139, [[1807.07915](#)].
- [139] CMS collaboration, A. M. Sirunyan et al., *Search for charged Higgs bosons in the  $H^\pm \rightarrow \tau^\pm \nu_\tau$  decay channel in proton-proton collisions at  $\sqrt{s} = 13$  TeV*, [JHEP](#) **07** (2019) 142, [[1903.04560](#)].
- [140] CMS collaboration, V. Khachatryan et al., *Search for light bosons in decays of the 125 GeV Higgs boson in proton-proton collisions at  $\sqrt{s} = 8$  TeV*, [JHEP](#) **10** (2017) 076, [[1701.02032](#)].
- [141] ALEPH, DELPHI, L3, OPAL, LEP collaboration, G. Abbiendi et al., *Search for Charged Higgs bosons: Combined Results Using LEP Data*, [Eur. Phys. J. C](#) **73** (2013) 2463, [[1301.6065](#)].
- [142] D. Hanneke, S. Fogwell and G. Gabrielse, *New Measurement of the Electron Magnetic Moment and the Fine Structure Constant*, [Phys. Rev. Lett.](#) **100** (2008) 120801, [[0801.1134](#)].
- [143] R. H. Parker, C. Yu, W. Zhong, B. Estey and H. Müller, *Measurement of the fine-structure constant as a test of the Standard Model*, [Science](#) **360** (2018) 191, [[1812.04130](#)].
- [144] L. Morel, Z. Yao, P. Cladé and S. Guellati-Khélifa, *Determination of the fine-structure constant with an accuracy of 81 parts per trillion*, [Nature](#) **588** (2020) 61–65.
- [145] T. Aoyama, T. Kinoshita and M. Nio, *Revised and Improved Value of the QED Tenth-Order Electron Anomalous Magnetic Moment*, [Phys. Rev. D](#) **97** (2018) 036001, [[1712.06060](#)].

- [146] S. Laporta, *High-precision calculation of the 4-loop contribution to the electron  $g - 2$  in QED*, [Phys. Lett. B](#) **772** (2017) 232–238, [[1704.06996](#)].
- [147] W. Yin and M. Yamaguchi, *Muon  $g - 2$  at multi-TeV muon collider*, [2012.03928](#).
- [148] E. J. Chun, S. Dwivedi, T. Mondal, B. Mukhopadhyaya and S. K. Rai, *Reconstructing heavy Higgs boson masses in a type X two-Higgs-doublet model with a light pseudoscalar particle*, [Phys. Rev. D](#) **98** (2018) 075008, [[1807.05379](#)].
- [149] E. J. Chun, S. Dwivedi, T. Mondal and B. Mukhopadhyaya, *Reconstructing a light pseudoscalar in the Type-X Two Higgs Doublet Model*, [Phys. Lett. B](#) **774** (2017) 20–25, [[1707.07928](#)].
- [150] S. Kanemura, K. Tsumura and H. Yokoya, *Multi-tau-lepton signatures at the LHC in the two Higgs doublet model*, [Phys. Rev. D](#) **85** (2012) 095001, [[1111.6089](#)].
- [151] M. Grazzini, S. Kallweit and D. Rathlev, *ZZ production at the LHC: fiducial cross sections and distributions in NNLO QCD*, [Phys. Lett. B](#) **750** (2015) 407–410, [[1507.06257](#)].
- [152] ATLAS collaboration, G. Aad et al., *Measurement of the ZZ Production Cross Section in pp Collisions at  $\sqrt{s} = 13$  TeV with the ATLAS Detector*, [Phys. Rev. Lett.](#) **116** (2016) 101801, [[1512.05314](#)].
- [153] ATLAS collaboration, M. Aaboud et al., *Measurement of fiducial and differential  $W^+W^-$  production cross-sections at  $\sqrt{s} = 13$  TeV with the ATLAS detector*, [Eur. Phys. J. C](#) **79** (2019) 884, [[1905.04242](#)].